A NEW SIMILARITY ANALYSIS OF THE TURBULENCE ENERGY SPECTRUM

by

Stephan Gamard

A thesis submitted to the
Department of Mechanical and Aerospace Engineering
and the Faculty of the Graduate School of the
State University of New York at Buffalo
in partial fulfillment of the requirements for the degree of

Master of Science

February 1999

The eternal mystery of the world is its comprehensibility.

-Albert Einstein

How can you be expected to govern a country that has 246 kinds of cheese?

-Charles De Gaulle

Abstract

A similarity analysis for the turbulence energy spectrum is proposed that extends Kolmogorov and Van Karman theories to include the effects of finite Reynolds number. From dimensional and physical considerations, a proper scaling is defined for low and high wavenumbers but with functions describing the entire range of the spectrum. The scaling for low wavenumbers implies the definition of an integral scale, L, based on the integral of the correlation function; this scale differs from the widely used scale $l \simeq u^3/\epsilon$.

The fact that both the scaled profiles describe the entire spectrum for finite values of Reynolds number but reduce to different profiles in the limit is used to determine their functional forms in the "overlap" region that both retain in the limit. The profiles in this region follow a power law with an exponent that is Reynolds number dependent but goes to $-5/3$ in the limit of infinite Reynolds number.

Existing models for low and high wavenumbers are modified to account for the Reynolds number dependence. They are then used to build a spectral model covering all the range of wavenumbers at every Reynolds number. This model allows us to get a better estimate of the exponent of the power law.

Experimental data from grid-generated turbulence are then examined and found to be in good agreement with the model.

Acknowledgments

I know it seems quite obvious, but I would like to start by thanking my advisor Dr. William K. George. Not only did he always help and guide me during all this work, but he also allowed me to realize one of my dreams with a week of sailing. He was like a father for me and his friendship will always be something I am looking for.

I wish also to thank all the personnel of the Mechanical and Aerospace Department who were always there to help me when I needed it, Dr. D. Taulbee and Dr. C. Madnia for being part of my committee, and L. Mydlarski and Z. Warhaft for sharing their results with me.

A special thought for my former school for allowing me to study in the USA (and for the French military service for not calling me too soon).

Last but not least, I would like to thank my family who always helped me to realize my dreams and supported me during all my life.

Contents

List of Figures

List of Tables

Nomenclature

A : Constant in the model of μ (equation 9.1)

A_1, A_2 : Constants in the model of the one-dimensional spectra near the origin

B_1, B_2, C_1

B : Constant in the low wavenumber model

B_{ij} : Velocity correlation tensor (equation 3.1)

C : Constant of proportionality for the spectrum in the inertial subrange

E : Energy spectrum (equation 3.6)

E_0 : Integration constant in the high wavenumber model

F_{ij}^1 : One-dimensional spectrum function (equation 3.5)

Longitudinal if $ij = 11$

Lateral if $ij = 22$

$\mathcal{F}_{ij}^1$: Half-line one-dimensional spectrum

f_H : Non-dimensional spectrum in high wavenumbers scaling (equation 5.3)

f_L : Non-dimensional spectrum in low wavenumbers scaling (equation 5.4)

g : $= R^{-5/3}\phi^{2/3}$, Ratio of f_L over f_H (equation 6.4)

h : Function modeling μ (equation 6.28)

k : Wavenumber

k_0 : Integration constant in the high wavenumber model

k_e : Wavenumber of reference in the low wavenumber model

k_n : Intermediate variable to define the overlap region

k_p : Wavenumber at which the dissipation integral gets its primary contribution

l : $\simeq u^3/\epsilon$, "Pseudo" integral scale

L : Physical integral scale: integral of the correlation function

L_p : Physical longitudinal integral scale (Batchelor's notation [2])

r : Space vector

S : Energy flux function (equation 5.10)

S_H : First term of a Taylor expansion of f_H at fixed Reynolds number (equation 6.7)

S_L : First term of a Taylor expansion of f_L at fixed Reynolds number (equation 6.6)

t : Time

T : Energy transfer between different wavenumbers

u : Turbulence velocity in isotropic case

u_i : Turbulence velocity

v : Alternative expression of u_2 in isotropic case

$\underline{x}$: Position vector

x : $= k/k_e$, variable in the low wavenumber model

Greek Symbols

α : Constant in the high wavenumber model

β : Constant in the model of μ (equation 9.1)

δ_{ij} : Kronecker symbol

γ : $= -5/3 + \mu$, exponent of the spectrum (equation 6.17)

Γ : Euler-Gamma function

ϵ : Dissipation rate (equation 3.25)

η : Kolmogorov microscale (equation 4.9)

λ : Taylor microscale (equation 4.10)

μ : Difference with $-5/3$ in the exponent of the spectrum (equation 6.24)

ν : Viscosity

ϕ : $=\epsilon L/u^3$, ratio of the integral length scales (equation 6.3)

Φ : Fourier transform of the velocity correlation tensor (equation 3.2)

$d\sigma$: Surface element

$d\theta$, $d\phi$: Elementary spherical coordinates

Nondimensional Parameters

R : $= L/\eta$, Reynolds number

R_L : $u.L/\nu$, Reynolds number based on the low wavenumbers parameters

R_λ : $u.\lambda/\nu$, Reynolds number based on u and the Taylor microscale

Subscripts

1 : Longitudinal direction

2 : Lateral direction

3 : Third direction

∞ : Value at infinite Reynolds number

H : High wavenumber

i, or j : Free index (the tensor notation is not used)

L : Low wavenumber

$\underline{x}$: Implies that x is a vector

Superscripts

1 : Dependence of the function only in the 1-direction

$\overline{x}$: Implies that x is non-dimensionalized in low wavenumbers scaling or, to take the average of x (chapter 3 only)

$\tilde{x}$: Implies that x is non-dimensionalized in high wavenumbers scaling

Relation Symbols

$\simeq$: "approximately equals to"

$\propto$: "proportional to"

Chapter 1

Introduction

1.1 Motivation

The year 1941 might be considered as the beginning of modern turbulence theory with three papers from Kolmogorov. With only three hypotheses (stated in chapter 1.2), Kolmogorov [20] produced physical evidence for turbulence similarity. After more than fifty years, his theory has been widely discussed and, apart from the question of universality, more or less accepted. However, a crucial point in Kolmogorov's theory is the necessity of "a sufficiently large Reynolds number". Unfortunately, this definition is rather unclear. So for the years that followed Kolmogorov papers, experimentalists tried to produce results at that "sufficiently large Reynolds number" which many claimed to have achieved, or to cover the gap in theory before those large Reynolds numbers.

In 1996, Mydlarski and Warhaft [25], proposed, on experimental grounds, that the exponent in the inertial subrange was not the $-5/3$ proposed by Kolmogorov, but rather a function of the Reynolds number that went to $-5/3$ in the limit of infinite Reynolds number. Meanwhile, George developed the Asymptotic Invariance Principle [10] and successfully applied it to a number of turbulent flows. The next step, which is presented in this thesis is to extend the Asymptotic Invariance Principle to

theoretically justify Warhaft's assumptions and lay down the first steps in expressing the similarity functions at low Reynolds numbers for the energy spectrum.

1.2 The Kolmogorov Hypotheses

Kolmogorov published three papers in 1941 concerning isotropic turbulence. Only the first one [20] (and to a certain extent the third one [19], which rederives the value of the exponent from the Navier-Stokes equations) are of interest to this work. We reproduce here a recent translation of the three hypotheses re-published in the Proceedings of the Royal Society as a special publication to mark the 50th anniversary of the original. We adapt the notations to the present work.

We start by giving the definition of *local isotropy*:

> "The turbulence is called locally isotropic in the domain G if it is homogeneous and if, besides, [the average properties of the flow] are invariant with respect to rotations and reflections of the original system of coordinate axes."

This definition was then followed by three hypotheses:

- The local isotropy

  > "(...) we think it is rather likely that in an arbitrary turbulent flow with a sufficiently large Reynolds number $R_L = uL/\nu$ the hypothesis of local isotropy is realized with good approximation in sufficiently small domains (...) not lying near the boundary of the flow or other singularities."

- First hypothesis of similarity

  > "For the locally isotropic turbulence the [statistics of the flow] are uniquely determined by the quantities ν and ϵ."

He then defines appropriate length to this domain (called the Kolmogorov scale, see chapter 4.2) and velocity scales. To determine the functional form of the two-points velocity correlations he adds a third hypothesis.

- Second hypothesis of similarity

> "If the [scales of the flow] are large in comparison with [the Kolmogorov scale], then the [statistics of the flow] are uniquely determined by the quantity ϵ and do not depend on ν."

The range of wavenumbers (in Fourier space) of validity of the latter hypothesis is called the inertial subrange. Note that Batchelor [2] includes both the inertial subrange and the dissipation range into the "universal equilibrium" range. Figure 1.1 describes the different regions in Fourier space. Based on these hypotheses, he determines that the two points velocity correlation function $B_{11}(r_1) \propto r_1^{2/3}$. A Fourier transform leads to the better known result $F_{11}^1 \propto k_1^{-5/3}$.

1.3 Thesis Outline

This section is a brief description of the present thesis. Chapter 2 gives an overview of the existing work on the subject. Since the amount of research on isotropic turbulence and the Kolmogorov hypotheses is quite overwhelming, we will restrain ourselves to the subjects dealing directly with our theory. The next chapter (chapter 3) is aiming to clearly define all the mathematical basis that we need. It defines among others the energy spectrum (chapter 3.1), the dissipation rate (chapter 3.4), and the half-line spectrum (3.5). Some isotropic properties are inserted (chapter 3.2) that lead to key relations between the different spectra (chapter 3.3). These isotropic simplifications are used only in the data analysis and are, thus, not required for the similarity theory.

As for any similarity theory, we require proper scalings, and thus length scales. Chapter 4 proposes that the appropriate length scale in low wavenumber should be

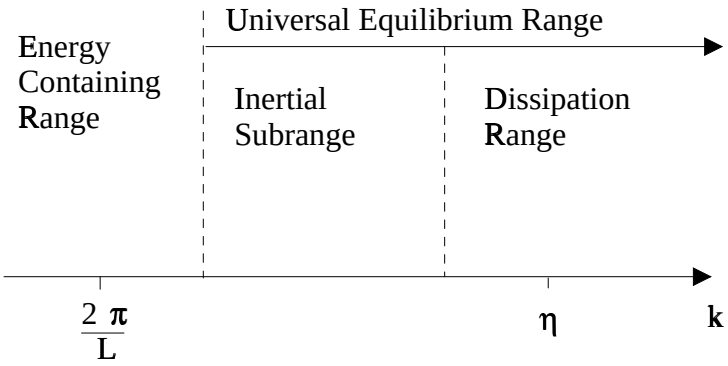

Figure 1.1: The different regions of turbulence

the physical integral scale (chapter 4.1), and not the widely used $l \simeq u^2/\epsilon$. Formulae to derive it from the spectra are also given. The second length scale has been first introduced by Kolmogorov and bears his name (chapter 4.2). It is representative of the small scales in turbulence corresponding to the high wavenumbers. Finally, as a reminder, we define the Taylor microscale (chapter 4.3). This scale is used here only in the experimental section since Reynolds numbers are formed on it.

The following chapter (5) develops the similarity analysis. We define the proper scalings for low and high wavenumbers (chapter 5.1), and justify them (chapter 5.2). The matching between the two profiles is used to derive the functional form in the overlap (chapter 6). The result yields a power law form with exponent $-5/3 + \mu(R)$, where μ is a function of the Reynolds number.

We then implement this theory on a set of grid-generated turbulence (chapter 7). First we check the isotropy of the experimental values (chapter 7.1) since we use isotropic simplifications later on. Then, the one-dimensional spectra are plotted in high (chapter 7.2) and low (chapter 7.3) wavenumbers scaling, before trying to obtain the experimental values for μ (chapter 7.4).

In order to refine the estimates of μ and especially its Reynolds number dependence, spectral models were developed (chapter 8) that should cover all the range of wavenumbers. From those, values of μ were obtained after a fit with the data sets. We first develop a low wavenumbers model (chapter 8.1), then one for the high wavenumbers region (chapter 8.2). Those models are then combined to form a composite model (chapter 8.3). The values of the exponent μ found this way proved to be quite similar to the ones found through data analysis only (chapter 8.4). It is important to note that the primary theory of this thesis does **not** depend on these models. While they are, of course, useful in other contexts, herein their purpose was to facilitate the determination of μ from the data.

Finally we summarize results on the exponent μ (chapter 9). A model for μ is proposed (chapter 9.1) that describes all the functional form of the profiles in the

overlap region. We then conclude the present work (chapter 10) and give some hints for future work on the subject.

Chapter 2

Previous Research

The energy spectrum and Kolmogorov theory are quite important subjects in the field of turbulence, so we will limit this section only to the materials directly related to the present work (or that can explain its evolution from earlier theories). An interested reader can easily find more information on the subject on books by Batchelor [2], Hinze [16], or Monin and Yaglom [24], or on an article by Bradshaw [3] that aims to clarify the studies of turbulence.

The study of turbulence is a recent one, but since the beginning people have tried to simplify the problem. Taylor was among the first to describe turbulence with the help of statistical tools and simplify it with isotropic hypotheses [30]. In this paper and those that followed it, he first introduced the correlation between the velocities at two points as a key function in the study of turbulence. Later on, he tried to see implications of spectral analysis [31], a tool that was only used by mathematicians at that time. Then, Von Karman and Howarth worked on the Navier-Stokes equation using product of two or three components of the velocity and derived what is now known as the energy equation. Von Karman also put forth the assumption of "self-preservation" which will form the basis of the low wavenumber scaling considered later. This hypothesis was not successful for physical reasons that became clear with Kolmogorov's work.

Kolmogorov developed in 1941 physical reasons for similarity with the publication of three papers. The first one [20] proposed an alternative definition of isotropy and gave three hypotheses that fully describe a similarity analysis at high Reynolds number. A questionable point was that Kolmogorov believed in the universality of the spectrum in the inertial range at high Reynolds number. Perhaps to avoid linking forever the problem of universality to its theory, he published another paper the same year [19] where he rederives the important results with the Navier-Stokes equation. Frisch [6] after emphasizing Landau's remark about the lack of universality, revisits Kolmogorov's theory from a symmetry point of view that apparently bypasses this problem.

The real importance of Kolmogorov's work was not appreciated in western countries before its revelation by Batchelor [2] in 1947. A special publication of the "Proceedings of the Royal Society of London" on the fiftieth anniversary of the Kolmogorov's theories re-publishes them in, along with papers, like the one from Hunt and Vassilicos [17] or the extension made by Frisch [5], commenting on their impact and the consequent evolution on turbulence works. The first implication of Kolmogorov hypotheses on the energy spectrum was developed by Obukhov in 1941 and leads to the fact that the energy spectrum follows a $-5/3$ power law in the inertial subrange. In 1962, Kolmogorov presented another paper [21] that takes into account the phenomenon of intermittency to modify his 1941 papers.

The following years, experimentalists affirmed having confirmed Kolmogorov results (see for instance Saddoughi's tests [29] and [28]), even though the Reynolds numbers were not that high. Thus the "$-5/3$-law" became widely accepted. Some theoreticians tried to fully define the Reynolds numbers evolution on the scalings and regions (see Von Karman and Lin [18]). In the meantime, some empirical models of the energy spectrum were developed, mostly at high wavenumbers by Corrsin, Pao [26] and [27], Lin [23], Hill [15] and others to catch the roll off in the dissipation range. For the low wavenumber range, the model from Von Karman is still used.

Then mixing of the models are sometimes used to create a model covering all the range of wavenumbers (see for instance Driscoll [4] or Helland *et al.* [14]).

In the perspective of the present work, an important breakthrough occurred in 1996 with the publication of the paper by Mydlarski and Warhaft [25]. They experimentally found a Reynolds number dependence in the exponent of the energy spectrum in the inertial range, contrary to earlier beliefs[1]. The exponent reaches the expected $-5/3$ only beyond a Reynolds number of 10^4.

Meanwhile, George and Hussein explained the problems of local isotropy by hypothesing that the turbulence is locally axisymmetric instead [13]. Then George and Gibson [12] showed that there can not be any universality in the spectrum since it depends on the initial conditions. This is emphasized with the basis for this present similarity analysis in George [8], or with consequences of self-preservation in different kind of turbulence [7]. The last step that directly leaded to this work was the development of the Asymptotic Invariance Principle to clearly defines a similarity analysis [9]. It was successfully applied to zero-pressure-gradient boundary layers (George and Castillo, 1997 [10]), turbulent pipes and channel flows (George, Castillo and Wosnik, 1997 [11]), and now to the the energy spectrum.

[1] These results were presented by Warhaft in Crete in June 1996 at a meeting also attended by George. He then informed Warhaft of the existence of the basis of this theory, but also of his lack of experimental data to verify it. Warhaft and Mydlarski, then shared their results to allow this thesis to be done.

Chapter 3

Definition of the Energy Spectrum and Direct Consequences

3.1 Definitions

The first step towards the definition of the energy spectrum is the velocity correlation tensor for two points separated by the space vector $\underline{r}$:

$$B_{ij}(\underline{r}) = \overline{u_i(\underline{x})u_j(\underline{x}+\underline{r})}. \tag{3.1}$$

We can then define (see Batchelor [2]) a spectral energy tensor by taking the Fourier transform of the velocity correlation tensor:

$$\Phi_{ij}(\underline{k}) = \frac{1}{8\pi^3}\iiint_{-\infty}^{\infty} e^{-i\underline{k}\cdot\underline{r}}\, B_{ij}(\underline{r})\, d\underline{r}, \tag{3.2}$$

or alternatively:

$$B_{ij}(\underline{r}) = \iiint_{-\infty}^{\infty} e^{i\underline{k}\cdot\underline{r}}\, \Phi_{ij}(\underline{k})\, d\underline{k}. \tag{3.3}$$

A consequence is that:

$$B_{ij}(0) = \overline{u_i(\underline{x})u_j(\underline{x})} = \iiint_{-\infty}^{\infty} \Phi_{ij}(\underline{k})\, d\underline{k}. \tag{3.4}$$

For experimental reasons, a Fourier analysis with respect to one-space coordinate only is sometimes considered. The resulting spectrum function is a one-dimensional Fourier transform of the velocity correlation tensor:

$$\begin{aligned} F_{ij}^1(k_1) &= \frac{1}{2\pi}\int_{-\infty}^{\infty} B_{ij}(r_1,0,0)\cdot e^{-ik_1r_1}\, dr_1 \\ &= \iint_{-\infty}^{\infty} \Phi_{ij}(k_1,k_2,k_3)\, dk_2\, dk_3. \end{aligned} \tag{3.5}$$

The superscript 1 in F_{ij}^1 is there to stress the fact that the dependence on the k_2 and k_3-directions vanishes by integration, leaving only a dependence on the k_1-direction. This new appellation with the 1-superscript is necessary since a function can not simply be named by its argument, in this case k_1.

In the case $i = j = 1$, $F_{ij}^1(k_1)$ is called the **longitudinal** one-dimensional spectrum, while $i = j = 2$ is the **lateral** one-dimensional spectrum.

Of considerable physical and theoretical interest is the energy spectrum, function defined by integrating the energy tensor Φ_{ii} over spherical shells of values k:

$$E(k) = \frac{1}{2}\int\int_{Sph.\, surface\, k=|k|} \Phi_{ii}(\underline{k})\, d\sigma(\underline{k}) \tag{3.6}$$

where $d\sigma = sin\theta\, d\phi\, d\theta$ in spherical polar coordinates. Note that $E(k)$ is a scalar function of only the magnitude $k = |k|$, hence the directional information has been removed.

A direct consequence of equation 3.6, which justifies its name "energy spectrum"

is that:

$$\sum_{i=1}^{3} \frac{\overline{u_i u_i}}{2} = \int_0^\infty E(k)\, dk. \tag{3.7}$$

3.2 Isotropic Turbulence

Since the first hypothesis of Kolmogorov states that in *small regions of space, the turbulence is nearly isotropic*, we will consider here only isotropic turbulence, although most of the conclusions probably have a much wider range of applicability.

For isotropic turbulence:

$$\overline{u_1^2} = \overline{u_2^2} = \overline{u_3^2} \equiv u^2. \tag{3.8}$$

Also, using isotropy, one can relate the energy spectrum $E(k)$ to the energy tensor $\Phi_{ij}(\underline{k})$ by:

$$\Phi_{ij}(\underline{k}) = \frac{E(k)}{4\pi k^4}(k^2\delta_{ij} - k_i k_j) \tag{3.9}$$

where δ_{ij} is the Kronecker symbol:

$$\delta_{ij} = \begin{cases} 1 & : \quad i = j \\ 0 & : \quad i \neq j \end{cases}$$

It is straightforward to derive the corresponding isotropic relations for the 1-dimensional spectra:

- longitudinal:

$$F_{11}^1(k_1) = \frac{1}{2}\int_{k_1}^\infty \left(1 - \left(\frac{k_1}{k}\right)^2\right) \cdot \frac{E(k)}{k}\, dk, \tag{3.10}$$

  or:

$$E(k) = k^3 \frac{d}{dk}\left(\frac{1}{k}\frac{dF_{11}^1(k)}{dk}\right). \tag{3.11}$$

- lateral:

$$\begin{aligned} F_{22}^1(k_1) &= \iint_{-\infty}^{\infty} \Phi_{22}(k_1,k_2,k_3)\,dk_2\,dk_3 \\ &= \frac{1}{4}\int_{k_1}^{\infty}\left(1+\left(\frac{k_1}{k}\right)^2\right)\cdot\frac{E(k)}{k}\,dk \\ &= \frac{1}{2}F_{11}^1 - \frac{1}{2}k_1\frac{dF_{11}^1}{dk_1}. \end{aligned} \tag{3.12}$$

3.3 Consequences of Isotropic Relations

As it will be shown in chapter 6, in the overlap region, the energy spectrum follows a power law: $E \propto k^n$. It follows from isotropic relations 3.11 and 3.12, that the exponent in the matching region is the same for all the spectra (three-dimensional, and one-dimensional), i.e.:

$$F_{11}^1 \propto k_1^n$$

and

$$F_{22}^1 \propto k_1^n$$

The isotropic relations also give relations between the different coefficients of proportionality. For example if

$$E = Ck^n \tag{3.13}$$

in the overlap region, we can express C_1 and C_2, where

$$F_{11}^1 = C_1 k_1^n \tag{3.14}$$

and

$$F_{22}^1 = C_2 k_1^n \tag{3.15}$$

by:

$$C_1 = \frac{C}{n(n-2)}, \tag{3.16}$$

and

$$C_2 = \frac{(n-1)C}{2n(2-n)}. \tag{3.17}$$

It then follows that in the region described by the power law, the ratio of the spectra is constant and given by:

$$\frac{F_{22}^1}{F_{11}^1} = \frac{1-n}{2}. \tag{3.18}$$

It will be seen in chapter 6 that $n = -5/3 + \mu(R)$ for finite Reynolds number and, in the limit of infinite Reynolds number, $\mu \to 0$ and $n \to -5/3$. Hence for finite Reynolds number the above relations become:

$$C_1 = \frac{C}{\left(\frac{5}{3}-\mu\right)\left(\frac{11}{3}-\mu\right)}, \tag{3.19}$$

$$C_2 = \frac{\left(-\frac{8}{3}+\mu\right)C}{\left(-\frac{10}{3}+2\mu\right)\left(\frac{11}{3}-\mu\right)}, \tag{3.20}$$

and

$$\frac{F_{22}^1}{F_{11}^1} = \frac{4}{3} - \frac{\mu}{2}. \tag{3.21}$$

They obviously reduce to the classical form for infinite Reynolds number, i.e.:

$$C_1 = \frac{9}{55}C, \tag{3.22}$$

$$C_2 = \frac{12}{55}C, \tag{3.23}$$

and:

$$\frac{F_{22}^1}{F_{11}^1} = \frac{4}{3}. \tag{3.24}$$

These relations will play an important role in constraining the empirical relations

in the experimental data analysis considered in chapter 7. We should note that, although Warhaft *et al.* [25] recognized equation 3.12, since they used equation 3.24, they appear to ignore the effect of this equation to relate the exponents of F_{11}^1 and F_{22}^1.

3.4 The Dissipation Rate

The wavenumbers at which viscous forces play an important part correspond to the values of k where the dissipation integral gets its primary contribution, and the integral in turn defines the dissipation rate ϵ. It is straightforward (see Batchelor [2]) to show that the rate of dissipation of turbulent kinetic energy per unit mass (or simply the dissipation rate) is related to the energy spectrum by:

$$\epsilon = 2\nu \int_0^\infty k^2 E(k)\, dk. \tag{3.25}$$

We use the isotropic relation between $E(k)$ and $F_{11}^1(k_1)$ (equation 3.11) to get ϵ as a function of the one-dimensional spectrum:

$$\epsilon = 30\nu \int_0^\infty k_1^2\, F_{11}^1(k_1)\, dk_1. \tag{3.26}$$

3.5 Half-Line versus Whole-Line Spectra

Experimentalists, for historical reasons, often prefer to deal with a half-line one-dimensional spectrum (which will be denoted by $\mathcal{F}_{ii}^1$ to differentiate it from the 1-D spectrum F_{ii}^1). This spectrum is simply the double of the 1-D spectrum (since the 1-D spectrum is symmetrical in k_1).

Theoreticians, on the other hand, prefer the whole-line spectrum because of its symmetry. Unfortunately, the distinction between the half-line and the one-dimensional spectrum is seldom defined in the literature and it is often difficult to decide which

one is used in a given result. This creates many more problems than simply dealing with the 1-D spectrum all along. Since the data set used to verify the present work was based on the half-line spectrum, I summarize below what our main equations become when using $\mathcal{F}_{ii}^1$.

- Isotropic relations with E:

$$\mathcal{F}_{11}^1 = \int_{k_1}^{\infty} \left(1 - \left(\frac{k_1}{k}\right)^2\right) \cdot \frac{E(k)}{k}\, dk \tag{3.27}$$

  and:

$$E(k) = \frac{1}{2} k^3 \frac{d}{dk} \left(\frac{1}{k} \frac{d\mathcal{F}_{11}^1(k)}{dk}\right). \tag{3.28}$$

- Isotropic relation with $\mathcal{F}_{22}^1$:

$$\mathcal{F}_{22}^1 = \frac{1}{2}\mathcal{F}_{11}^1 - \frac{1}{2} k_1 \frac{d\mathcal{F}_{11}^1}{dk_1}. \tag{3.29}$$

- Dissipation rate:

$$\epsilon = 15\nu \int_0^{\infty} k_1^2\, \mathcal{F}_{11}^1(k_1)\, dk_1. \tag{3.30}$$

- Longitudinal velocity:

$$\begin{aligned} u^2 &= B_{11}(0) \\ &= \int_{-\infty}^{\infty} F_{11}^1\, dk_1 \\ &= 2 \cdot \int_0^{\infty} F_{11}^1\, dk_1 \\ &= \int_0^{\infty} \mathcal{F}_{11}^1\, dk_1. \end{aligned} \tag{3.31}$$

Chapter 4

The Length Scales

4.1 The Integral Length Scale

There exists much confusion in the literature about which scales are really appropriate to the description of the energy spectrum. Nonetheless, all agree in the need of a large scale for turbulence. The large scale we consider will be called **physical integral scale** and represented by L [1]. It is defined from the integral of the correlation function. It is important to note that the "physical" integral scale differs from the "pseudo" integral scale ($l \simeq u^3/\epsilon$) often found in the literature. In fact, the ratio $L/l = \epsilon L/u^3$ $(= \phi)$ is Reynolds-number dependent and constant only in the limit of infinite Reynolds number (see George [8]). Recognizing the difference between L and l is fundamental in understanding the following theory and the interpretation of the data.

The physical integral scale is not unique since, even in isotropic turbulence, there are still longitudinal and lateral correlation functions. For the energy spectrum E, we will use L_1, the longitudinal integral scale (called L_p in Batchelor's [2]). This longitudinal integral scale, and its counterpart, L_2, the transverse integral scale can be related to the spectra by:

[1] with the appropriate subscript to precisely distinguish which integral scale is being referred to.

- Longitudinal 1-dimensional spectrum:

$$L_1 = \frac{\int_0^\infty B_{11}(r)\,dr}{B_{11}(0)}. \tag{4.1}$$

- Lateral 1-dimensional spectrum:

$$L_2 = \frac{\int_0^\infty B_{22}(r)\,dr}{B_{22}(0)}. \tag{4.2}$$

The integral scale can also be expressed in terms of the 1-dimensional spectrum. In equation 4.1, we replace $B_{11}(0)$:

$$B_{11}(0) = u^2 = \int_{-\infty}^{\infty} F_{11}^1(k_1)\,dk_1,$$

then, using relation 3.5, we get:

$$F_{11}^1(0) = \frac{1}{2\pi}\int_{-\infty}^{\infty} B_{11}(r)\,dr = \frac{1}{\pi}\int_0^\infty B_{11}(r)\,dr,$$

implying finally:

$$L_1 = \pi\frac{F_{11}^1(0)}{\int_{-\infty}^{\infty} F_{11}^1(k_1)\,dk_1}. \tag{4.3}$$

Similarly,

$$L_2 = \pi\frac{F_{22}^1(0)}{\int_{-\infty}^{\infty} F_{22}^1(k_1)\,dk_1}. \tag{4.4}$$

The relation that has been used to derive the integral scale in the experimental part of this work with the half-line spectrum is:

$$L_1 = \frac{\pi}{2}\frac{\mathcal{F}_{11}^1(0)}{\int_0^{\infty} \mathcal{F}_{11}^1(k_1)\,dk_1}. \tag{4.5}$$

The same kind of relation can be derived for the lateral 1-dimensional spectrum:

$$L_2 = \frac{\pi}{2} \frac{\mathcal{F}_{22}^1(0)}{\int_0^\infty \mathcal{F}_{22}^1(k_1)\, dk_1}. \tag{4.6}$$

Using isotropic relations, it is straightforward to show that:

$$L_1 = \frac{3\pi}{4} \frac{\int_0^\infty E(k)/k\, dk}{\int_0^\infty E(k)\, dk} \tag{4.7}$$

and:

$$\frac{L_2}{L_1} = \frac{1}{2}. \tag{4.8}$$

This last equation is a consequence of isotropy **only** and does not depend on any other property of the spectrum. In the data analysis considered later (chapter 7), it will, in fact, be seen to be the least well-satisfied of the isotropic conditions considered.

4.2 The Kolmogorov Microscale

The other important length scale is the Kolmogorov microscale (η). Based on Kolmogorov second hypothesis, which implies that the important parameters in the equilibrium range are ϵ and ν, we define (on dimensional basis) a microscale:

$$\eta = \left(\frac{\nu^3}{\epsilon} \right)^{\frac{1}{4}}. \tag{4.9}$$

This scale is characteristic of the high wavenumber part of the spectrum since it is of the order of the smallest eddies found in homogeneous turbulence.

4.3 The Taylor Microscale

The last length scale of interest is called the Taylor microscale (λ). As for the other length scales, we can define two λ, one for each one-dimensional spectrum. The one for the longitudinal is given by:

$$-\frac{1}{\lambda_1^2} = \frac{1}{u^2}\left.\frac{d^2 B_{11}}{dr^2}\right|_{r=0}. \tag{4.10}$$

The behavior of the correlation function near the origin is then approximated by:

$$B_{11}(r) \simeq u^2\left(1 - \frac{r^2}{2\lambda_1^2}\right). \tag{4.11}$$

We can then easily relate the Taylor microscale to the 1-D longitudinal and the energy spectra by:

$$\begin{aligned}\lambda_1^2 &= \frac{u^2}{\int_{-\infty}^{\infty} k_1^2 F_{11}^1(k_1)\,dk_1} \\ &= \frac{15\cdot u^2}{2\cdot\int_0^{\infty} k^2 E(k)\,dk} \\ &= 5\frac{\int_0^{\infty} E(k)\,dk}{\int_0^{\infty} k^2 E(k)\,dk}.\end{aligned} \tag{4.12}$$

The same way, we define it for the lateral one-dimensional spectrum:

$$-\frac{1}{\lambda_2^2} = \frac{1}{v^2}\left.\frac{d^2 B_{22}}{dr^2}\right|_{r=0}, \tag{4.13}$$

so that

$$\lambda_2^2 = \frac{v^2}{\int_{-\infty}^{\infty} k_1^2 F_{22}^1(k_1)\,dk_1} \tag{4.14}$$

This scale appears in this work only in the experimental part with the half-line

spectrum, so:

$$\begin{aligned} \lambda_1^2 &= \frac{u^2}{\int_0^\infty k_1^2 \mathcal{F}_{11}^1(k_1)\, dk_1} \\ \lambda_2^2 &= \frac{v^2}{\int_0^\infty k_1^2 \mathcal{F}_{22}^1(k_1)\, dk_1}. \end{aligned}$$

Using isotropic relation 3.12, it is easy to show that:

$$\frac{\lambda_2^2}{\lambda_1^2} = \frac{1}{2}. \tag{4.15}$$

Chapter 5

Similarity Considerations

Following George [8], we will argue in term of the energy equation:

$$\frac{\partial E(k)}{\partial t} = T(k) - 2\nu k^2 E(k) \tag{5.1}$$

that relates the temporal variation of the energy spectrum in terms of itself and T, the energy transfer between different wavenumbers. A discussion on the two different regions and scalings have also been treated by Von Karman and Lin [18] or in Tennekes and Lumley [32].

5.1 Similarity Scalings

A dimensional analysis of the energy spectrum shows its proportionality to the product of a characteristic velocity and length. As seen in chapter 4, we can associate a length and velocity scale to the two regions of interest: L, u for the low and η, $u_\eta = (\nu.\epsilon)^{1/4}$ for the high wavenumbers part of the spectrum. Based on the ratio of the length scales, we define a Reynolds number, R, given by:

$$R = \frac{L}{\eta}. \tag{5.2}$$

The spectra can be scaled by either set of parameters, but will retain a Reynolds number dependence. Using ϵ and η, a dimensional analysis yields:

$$\tilde{E} = f_H(\tilde{k}, R) \tag{5.3}$$

with:

$$\begin{aligned} \tilde{k} &= k\eta \\ \tilde{E}(\tilde{k}, R) &= \frac{E(\tilde{k}, R)}{(\epsilon\nu^5)^{1/4}}. \end{aligned}$$

Using u and L, a dimensional analysis yields:

$$\overline{E} = f_L(\overline{k}, R) \tag{5.4}$$

with:

$$\begin{aligned} \overline{k} &= kL \\ \overline{E}(\overline{k}, R) &= \frac{E(\overline{k}, R)}{u^2 L}. \end{aligned}$$

The tilta represents a non-dimensional scaling in high wavenumbers and the over-bar one in low wavenumbers.

It is important to note that both f_L and f_H represent exactly the same spectrum, they are just the non-dimensional results of different scalings of the same function, at least at finite Reynolds number. However, in the limit of infinite Reynolds number, f_H reduces to the Kolmogorov scaling and loses the ability to collapse the low wavenumber spectral behavior. Similarly f_L reduces to the Von Karman spectral scaling and loses the ability to collapse the dissipation range. In fact, at low wavenumbers, $f_H \propto \tilde{k}^{-5/3}$ while for high wavenumbers $f_L \propto \overline{k}^{-5/3}$. This is the reason for including the parameter R in $\overline{E}(\overline{k}, R)$ and $\tilde{E}(\tilde{k}, R)$. Obviously this dependence

vanishes in the limit of infinite Reynolds number so that:

$$\lim_{R\to\infty} \overline{E}(\overline{k}, R) = \overline{E}_\infty(\overline{k}) \quad \text{only}$$
$$\lim_{R\to\infty} \tilde{E}(\tilde{k}, R) = \tilde{E}_\infty(\tilde{k}) \quad \text{only}$$

Therefore, $\overline{E}_\infty(\overline{k})$ and $\tilde{E}_\infty(\tilde{k})$ can not have the same functional dependence on k, except in a possible overlap region (the $k^{-5/3}$ region).

It is often thought that f_H is a universal function independent of the flow. However as seen in George [8] and repeated here, we can relate the two non-dimensionalised scaling expressions. Since they represent the same spectrum at finite Reynolds number, it follows that:

$$f_L(\overline{k}, R) = R^{-5/3}\, \phi^{2/3}\, f_H(\tilde{k}, R) \tag{5.5}$$

Obviously, both depend on the Reynolds number.

5.2 Physical Analysis

We now aim to explain the limiting behavior of $\overline{E}_\infty(\overline{k})$ and $\tilde{E}_\infty(\tilde{k})$ by splitting the spectral energy equation into two parts: one for the low wavenumbers, say $(0, k_p)$, and the other for the high wavenumbers, say (k_p, ∞). k_p will have a specific definition later, for now it can be considered as a wavenumber in a medium range.

Using the scalings defined before, one can change the energy equation 5.1 into two non-dimensional versions:

- for low wavenumbers:

$$\frac{\partial \overline{E}(\overline{k}, R)}{\partial \overline{t}} = \overline{T}(\overline{k}, R) - \frac{2}{R_L}\overline{k}^2 \overline{E}(\overline{k}, R) \tag{5.6}$$

$R_L = u.L/\nu$ is a Reynolds number based on the integral scale.

- for high wavenumbers:

$$\frac{\partial \tilde{E}(\tilde{k},R)}{\partial \tilde{t}} = \tilde{T}(\tilde{k},R) - 2\tilde{k}^2\tilde{E}(\tilde{k},R) \tag{5.7}$$

If the Reynolds number $R = L/\eta$ is sufficiently high and k_p is chosen between L^{-1} and η^{-1} so that $\overline{k} \gg 1$ and $\tilde{k} \ll 1$, then the resulting equations are (in **dimensional form**):

$$\frac{\partial E(k)}{\partial t} \simeq T(k) \qquad (0 < k < k_p) \tag{5.8}$$

$$0 \simeq T(k) - 2\nu k^2 E(k) \quad (k_p < k < \infty). \tag{5.9}$$

Equation 5.8 is approximately valid for low wavenumbers and equation 5.9 for the high ones. These two equations become exact only in the limit of an infinite Reynolds number. Their physical interpretations are that the low wavenumber region has no direct dissipation and loses energy only by the spectral energy transfer T at high wavenumbers. All the dissipation occurs at high wavenumbers which are in statistical equilibrium (hence Batchelor's [2] designation of it as the "universal equilibrium range"). These energy-containing and dissipation ranges are only completely separated at infinite Reynolds number.

We now examine the two regions for finite R. We first define S, the energy flux function:

$$\frac{dS}{dk} = -T. \tag{5.10}$$

For the low wavenumber region, i.e. for $k < k_p$, we integrate equation 5.8:

$$\frac{d}{dt}\int_0^{k_p} E\, dk \simeq \int_0^{k_p} T\, dk, \tag{5.11}$$

or using the fact that almost all the energy is contained in this region,

$$\frac{3}{2}\frac{du^2}{dt} \simeq -S. \tag{5.12}$$

For the high wavenumber region, $k > k_p$, we integrate equation 5.9:

$$0 \simeq \int_{k_p}^{\infty} T\,dk - 2\nu \int_{k_p}^{\infty} k^2 E dk. \tag{5.13}$$

Knowing that $\int_0^{\infty} T\,dk = 0$, we simplify equation 5.13:

$$0 \simeq S - 2\nu \int_{k_p}^{\infty} k^2 E dk. \tag{5.14}$$

Now in the limit of infinite Reynolds number, the above equations are exact, then k_p is the wavenumber at which the dissipation integral gets its primary contribution, and thus $S = \epsilon$ as defined in chapter 3.4. We note that for low wavenumbers the important parameters are u and ϵ and, for high wavenumbers, ν and ϵ. Since this is only valid at infinite Reynolds number, neither scaling is expected to perfectly collapse the data anywhere; the low wavenumber region will still dissipate energy, and the high wavenumber region still contains some of it.

Chapter 6

Matching of the Two Profiles

Since the spectrum both in low and high wavenumber scalings is a non-dimensional profile with different scales and the ratio of those scales is Reynolds number dependent, then there can not exist any region in between which would be Reynolds number independent (except possibly in the limit of infinite Reynolds number).

f_L and f_H represent the spectrum everywhere (for finite Reynolds number), and so, the problem of solving the overlap region should be tackled in a different way than the usual: we do not try to see if f_L and f_H overlap and match them if they do, but we rather see how the fact that those finite Reynolds number functions degenerate in different ways at infinite Reynolds number can be used to determine their functional form in the common region they describe in this limit. All this methodology has been developed in George and Castillo (1997)[10] and is also found in George, Castillo and Wosnik (1997)[11] and adapted to the present theory.

Even if we do not know the analytical form of f_L and f_H, we can still use their properties. First, since even with two different scalings, we describe the same spectrum, then, from equations 5.3 and 5.4:

$$u^2 L\, f_L(\overline{k}, R) = (\epsilon\nu^5)^{1/4}\, f_H(\tilde{k}, R)$$

$$f_L(\overline{k}, R) = R^{-5/3}\,\phi^{2/3}\,f_H(\tilde{k}, R), \tag{6.1}$$

where R is defined as the ratio of the scaling length scales:

$$R = \frac{L}{\eta}, \tag{6.2}$$

and

$$\phi = \frac{\epsilon L}{u^3}. \tag{6.3}$$

As noted in section 4.1, ϕ is the ratio of the "physical" length scale, L, over the "pseudo" length scale, l.

To simplify the following expressions, we define g as:

$$g(R) = R^{-5/3}\,\phi^{2/3}. \tag{6.4}$$

Then, for finite values of R, partial derivatives from both high and low wavenumbers forms of the spectrum must be the same, implying:

$$\begin{aligned} \frac{\partial}{\partial k}\left((u^2 L) f_L(\overline{k}, R)\right)\Big|_R &= \frac{\partial}{\partial k}\left((\epsilon\nu^5)^{1/4} f_H(\tilde{k}, R)\right)\Big|_R \\ L(u^2 L)\,\frac{\partial f_L(\overline{k}, R)}{\partial \overline{k}}\Big|_R &= \eta(\epsilon\nu^5)^{1/4}\,\frac{\partial f_H(\tilde{k}, R)}{\partial \overline{k}}\Big|_R . \end{aligned}$$

Therefore:

$$\frac{\overline{k}}{f_L}\,\frac{\partial f_L}{\partial \overline{k}}\Big|_R = \frac{\tilde{k}}{f_H}\,\frac{\partial f_H}{\partial \tilde{k}}\Big|_R . \tag{6.5}$$

Finally, in the limit, both f_L and f_H should become asymptotically independent of R:

$$\begin{aligned} f_L(\overline{k}, R) &\to f_{L\infty}(\overline{k}) \quad \text{only} \\ f_H(\tilde{k}, R) &\to f_{H\infty}(\tilde{k}) \quad \text{only} \end{aligned}$$

when $R \to \infty$.

In the limit of infinite Reynolds number, the question is to know if we still have a common part to the two different scalings, in other words, is there any region where equation 6.1 is valid? To examine this, we look how f_L and f_H are changing with R with a Taylor expansion at fixed k:

$$\frac{f_L(\overline{k}, R + \Delta R) - f_L(\overline{k}, R)}{\Delta R\, f_L(\overline{k}, R)} \simeq \frac{1}{f_L(\overline{k}, R)} \left.\frac{\partial f_L(\overline{k}, R)}{\partial R}\right|_{\overline{k}} = S_L(\overline{k}, R), \tag{6.6}$$

and:

$$\frac{f_H(\tilde{k}, R + \Delta R) - f_H(\tilde{k}, R)}{\Delta R\, f_H(\tilde{k}, R)} \simeq \frac{1}{f_H(\tilde{k}, R)} \left.\frac{\partial f_H(\tilde{k}, R)}{\partial R}\right|_{\tilde{k}} = S_H(\tilde{k}, R). \tag{6.7}$$

S_L and S_H represent the Reynolds number dependence in f_L and f_H thus:

$$\lim_{R\to\infty} S_L(\overline{k}, R) = 0 \quad , \tag{6.8}$$

$$\lim_{R\to\infty} S_H(\tilde{k}, R) = 0 \quad . \tag{6.9}$$

We want to examine if there is an matching region when $R \to \infty$, which would correspond to:

$$\begin{cases} \overline{k} & \to & \infty \\ \tilde{k} & \to & 0 \end{cases}$$

Since $\overline{k}/\tilde{k} = R$, in order to fix our interest in the overlap region, should it exist, we define an intermediate variable: $k_n = \overline{k} \cdot R^{-n}$, where n is to be defined. We can simultaneously satisfy $\overline{k} \to \infty$ and $\tilde{k} \to 0$ as $R \to \infty$ if we choose:

$$\begin{aligned} \tilde{k} &= \overline{k} \cdot R^{-1} \\ &= k_n \cdot R^{n-1}, \end{aligned} \tag{6.10}$$

which require $0 < n < 1$.

Introducing k_n in equation 6.1:

$$f_L(\overbrace{k_n R^n}^{\overline{k}}, R) = g(R)\, f_H(\overbrace{k_n R^{n-1}}^{\tilde{k}}, R), \tag{6.11}$$

we can differentiate with respect to R at fixed k_n to obtain:

$$\left.\frac{\partial f_L}{\partial \overline{k}}\right|_R \left.\frac{\partial \overline{k}}{\partial R}\right|_{k_n} + \left.\frac{\partial f_L}{\partial R}\right|_{\overline{k}} = \frac{dg}{dR} f_H + g\left[\left.\frac{\partial f_H}{\partial \tilde{k}}\right|_R \left.\frac{\partial \tilde{k}}{\partial R}\right|_{k_n} + \left.\frac{\partial f_H}{\partial R}\right|_{\tilde{k}}\right]. \tag{6.12}$$

Using equation 6.10:

$$n\frac{\overline{k}}{R}\left.\frac{\partial f_L}{\partial \overline{k}}\right|_R + \left.\frac{\partial f_L}{\partial R}\right|_{\overline{k}} = \frac{dg}{dR} f_H + g\left[(n-1)\frac{\tilde{k}}{R}\left.\frac{\partial f_H}{\partial \tilde{k}}\right|_R + \left.\frac{\partial f_H}{\partial R}\right|_{\tilde{k}}\right]. \tag{6.13}$$

We multiply by: $R/f_L = R/(g \cdot f_H)$:

$$n\frac{\overline{k}}{f_L}\left.\frac{\partial f_L}{\partial \overline{k}}\right|_R - (n-1)\frac{\tilde{k}}{f_H}\left.\frac{\partial f_H}{\partial \tilde{k}}\right|_R = \frac{R}{g}\frac{dg}{dR} + R\left[\frac{1}{f_H}\left.\frac{\partial f_H}{\partial R}\right|_{\tilde{k}} - \frac{1}{f_L}\left.\frac{\partial f_L}{\partial R}\right|_{\overline{k}}\right]. \tag{6.14}$$

Combining this equation with equation 6.5, we finally obtain :

$$\frac{\tilde{k}}{f_H}\left.\frac{\partial f_H}{\partial \tilde{k}}\right|_R = \frac{R}{g}\frac{dg}{dR} + R\left[\frac{1}{f_H}\left.\frac{\partial f_H}{\partial R}\right|_{\tilde{k}} - \frac{1}{f_L}\left.\frac{\partial f_L}{\partial R}\right|_{\overline{k}}\right], \tag{6.15}$$

or:

$$\frac{\tilde{k}}{f_H}\left.\frac{\partial f_H}{\partial \tilde{k}}\right|_R = \gamma(R) + R[S_H(\tilde{k}, R) - S_L(\overline{k}, R)], \tag{6.16}$$

where $\gamma(R)$ is defined by:

$$\gamma(R) = \frac{R}{g}\frac{dg}{dR} = \frac{d(\ln g)}{d\ln R}. \tag{6.17}$$

All the dependence in k in equation 6.16 is in the $R[S_H(\tilde{k}, R) - S_L(\overline{k}, R)]$ term.

Now if:

$$R|S_H| \ll \gamma, \tag{6.18}$$

and:

$$R|S_L| \ll \gamma, \tag{6.19}$$

then γ dominates on the right-hand side of equation 6.16. Another weaker condition is that $S_L = S_H$, mainly that both scaling profiles have the same dependence in R.

Therefore, as a first order approximation, we neglect $(S_H - S_L)$ on $\gamma(R)$ and get:

$$\left.\frac{\overline{k}}{f_L}\frac{\partial f_L}{\partial \overline{k}}\right|_R = \gamma(R), \tag{6.20}$$

$$\left.\frac{\tilde{k}}{f_H}\frac{\partial f_H}{\partial \tilde{k}}\right|_R = \gamma(R). \tag{6.21}$$

Here the functions are first-order approximations only, higher order terms being neglected. Note that it is different from an expansion at infinite Reynolds number where γ would have to be constant. Obviously the approximation is valid only as long as $R[S_H - S_L] \ll \gamma$, a condition which limits the matching region.

An immediate consequence of integrating equations 6.20 and 6.21 leads to a power law for both f_L and f_H:

$$f_L(\overline{k}, R) = C_L(R) \cdot (\overline{k})^{\gamma(R)} \tag{6.22}$$

$$f_H(\tilde{k}, R) = C_H(R) \cdot (\tilde{k})^{\gamma(R)} \tag{6.23}$$

Note: to be fully accurate, we should have $(\overline{k}+\overline{a})^{\gamma(R)}$ instead of simply $(\overline{k})^{\gamma(R)}$ where $\overline{a}$ is a constant resulting from the integration. However, based on experimental reasons, this term has never been observed, we assume its value to be zero. (this implies the integration constant for f_H to be null also).

Using the definition of g (equation 6.4) into equation 6.17 leads to the value of $\gamma_\infty = -5/3$, which is the result predicted by Kolmogorov hypotheses. We then define μ to be:

$$\mu = \gamma - \gamma_\infty = \gamma + 5/3. \tag{6.24}$$

By taking the ratio of f_L over f_H, we get g:

$$g(R) = \frac{f_L}{f_H} = \frac{C_L(R)}{C_H(R)} R^{-5/3+\mu(R)} \tag{6.25}$$

Going back to the definition of $\gamma(R)$ (equation 6.17) and combining it with equation 6.25 yield:

$$\ln R \frac{d\gamma}{d\ln R} = \frac{d \ln C_H/C_L}{d \ln R}, \tag{6.26}$$

which has as solution

$$\frac{C_H}{C_L} = \exp\left[(\mu(R)) \ln R + h\right], \tag{6.27}$$

where h is linked to μ by:

$$\mu(R) = -\frac{dh}{d\ln R}. \tag{6.28}$$

(this relation comes from putting C_H/C_L from equation 6.27 into equation 6.26.)

So the determination of h allows the determination of all our functions. Indeed,

$$\begin{aligned} g(R) &= \frac{C_L}{C_H} R^{-5/3+\mu(R)} \\ &= \exp\left[-\mu \ln R - h + (-5/3 + \mu) \ln R\right] \\ &= \exp\left[-5/3 \ln R - h\right] \end{aligned} \tag{6.29}$$

C_H and C_L must become finite and different from zero in the limit of infinite Reynolds number. Otherwise the spectrum would increase without any limit, which is not physically acceptable, or there could be no inertial subrange at infinite Reynolds number (if $C_{H\infty}$ and $C_{L\infty}$ are null). So to avoid that, we must have either:

- C_H, C_L stay constant, and $\mu = 0$ and are, thus, Reynolds number independent.

Or:

- $\mu \to 0$ faster than $\ln R \to \infty$ and $h(R) \to h_\infty = constant$, which immediately implies that:

$$\frac{C_{H\infty}}{C_{L\infty}} = \exp h_\infty \tag{6.30}$$

The first condition leads to a $-5/3$ power-law which is independent of Reynolds number. However, as shown by Mydlarski and Warhaft (1996) [25], the exponent is Reynolds-number dependent. We therefore conclude that this hypothesis is not valid.

In conclusion, once h is defined, then the spectrum is completely defined in the overlap region at every Reynolds number.

Chapter 7

Analysis of the Spectral Data

In order to verify the above theory, we need to use nearly isotropic turbulence data over a wide range of Reynolds number. Ideally, to fully test the theory, the data sets should be obtained with the same initial conditions since George 1989 [7] or George and Gibson 1992 [12] showed they highly influence the functional forms. Such data does not exist at the moment, we therefore used the spectral data (longitudinal and lateral one-dimensional spectrum) obtained by Mydlarski and Warhaft (1996) [25] obtained in a careful series of experiments. Briefly the experiments were performed downstream of a variety of passive and active grids. The turbulence was effectively homogeneous across the flow and decayed slowly downstream. The details of their installation will not be repeated here since it is not essential to the present work; the curious reader can refer to their paper for more information.

Table 7.1: Testing Parameters

R_λ	**50**	**100**	**124**	**174**	**207**	**275**	**330**	**473**
Modes	static grid		active grid					
ϵ $(m^2 s^{-3})$	0.227	0.071	0.329	1.42	3.27	1.75	5.15	15.3
η (mm)	0.349	0.467	0.318	0.221	0.179	0.210	0.160	0.122
$\mathbf{u^2}$ $(m^2 s^{-2})$	0.0235	0.0242	0.0715	0.2067	0.3751	0.3636	0.7483	1.8526
$\mathbf{v^2}$ $(m^2 s^{-2})$	0.0195	0.0221	0.0598	0.1877	0.3212	0.2516	0.6497	1.3815

Table 7.2: Isotropy checked

R_ν	$\mathbf{u^2}$ (m^2s^{-2})	$\mathbf{v^2}$ (m^2s^{-2})	$\mathbf{u^2/v^2}$	$\mathbf{L_1/L_2}$	$\boldsymbol{\lambda_1^2/\lambda_2^2}$
50	0.0234	0.0196	1.20	2.96	2.09
100	0.0243	0.0221	1.10	3.04	2.01
124	0.0715	0.0598	1.20	2.46	1.93
174	0.2067	0.1877	1.01	2.95	1.56
207	0.3751	0.3212	1.17	2.52	1.74
275	0.3633	0.2516	1.44	3.94	2.10
330	0.7483	0.6497	1.15	2.96	1.58
473	1.8526	1.3814	1.34	3.06	1.73

Those tests were performed on quite a wide range of Reynolds number; unfortunately they were not performed with strictly identical initial conditions and this is apparent in what follows. The important experimental parameters are listed in table 7.1.

It should be noted that all the data sets have been done with the half-line spectrum.

7.1 On the Isotropy of the Spectrum

We used isotropic simplifications whenever possible in this theory. So, before applying our results to a data set, we checked to see if it was legitimate to use isotropic assumptions. This was tested in many ways to assure its veracity. Results of our calculations are in table 7.2.

First, we checked relation 3.21 by plotting F_{22}^1/F_{11}^1 and $4/3 - \mu/2$. If the set is isotropic, we should see a constant region on the curve F_{22}^1/F_{11}^1 vs. k_1 corresponding to a power law region. An example is given in figure 7.1.

Then, we checked the ratio of $\overline{u_1^2}$ over $\overline{u_2^2}$. The results have proved to be quite good. We then checked the large scales by computing L_1/L_2. The set is isotropic if the ratio is equal to 2 (equation 4.8). This test was less successful, since the values

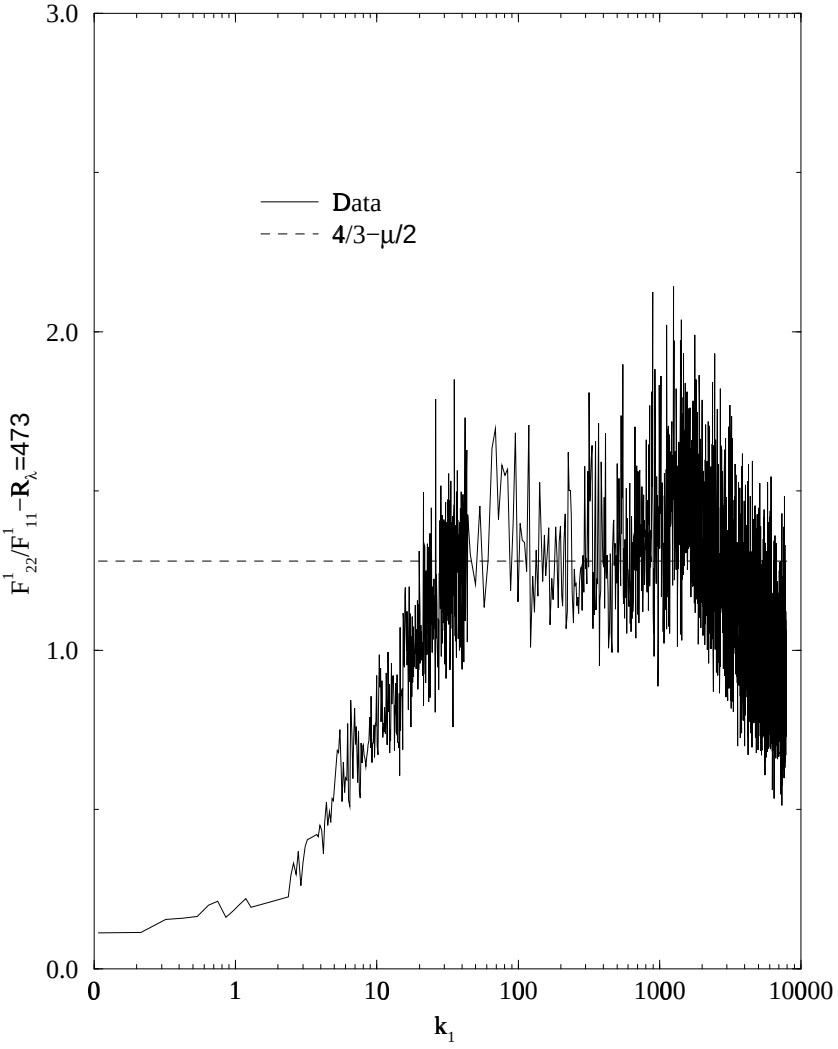

Figure 7.1: Isotropic test between F^1_{11} and F^1_{22} at $R_\lambda = 473$

were between 20 and 50% off, implying a lack of isotropy in the large scales. The values of the ratios λ_1^2/λ_2^2 were for the most part close to the value of 2 expected from equation 4.15, confirming that the smaller scales were close to being isotropic. We can note that the value of ϵ cited by Mydlarski and Warhaft [25] were consistent with those obtained by integrating $k_1^2.\mathcal{F}_{11}^1$ (equation 3.30), and this integral is part of the definition of λ_1 (equation 4.15).

In conclusion, the data can, with restrictions, be considered as isotropic, the main deviation occurring at large scales. However, this did not affect plots in low wavenumbers scaling as seen in chapter 7.3. The set at $R_\lambda = 275$ is the least isotropic one at every scale, which certainly explains the problem in obtaining μ with the composite model developed later in chapter 8.

7.2 The High Wavenumber Scaling

This is the classical Kolmogorov scaling (equation 5.3), which has proven to be quite successful on many experiments. As expected, we see (figure 7.2) a tendency towards collapse except at low wavenumbers where the scaling in no longer appropriate. The increase of the spectrum, at low wavenumbers, with the Reynolds number is also expected. Unfortunately, the difference between the initial conditions is probably responsible for the lack of a consistent trend with Reynolds numbers at low wavenumbers.

Some can say that those figures show nearly 2 decades of $-5/3$ power law region for the highest Reynolds number; but when the spectrum is multiplied by $\tilde{k}^{5/3}$ (see figure 7.3 for the highest number), Mydlarski and Warhaft [25] did not observe the flat region which would have been implied by a $-5/3$ power law, nor do we when re-plotting the same data. This is consistent with our theory.

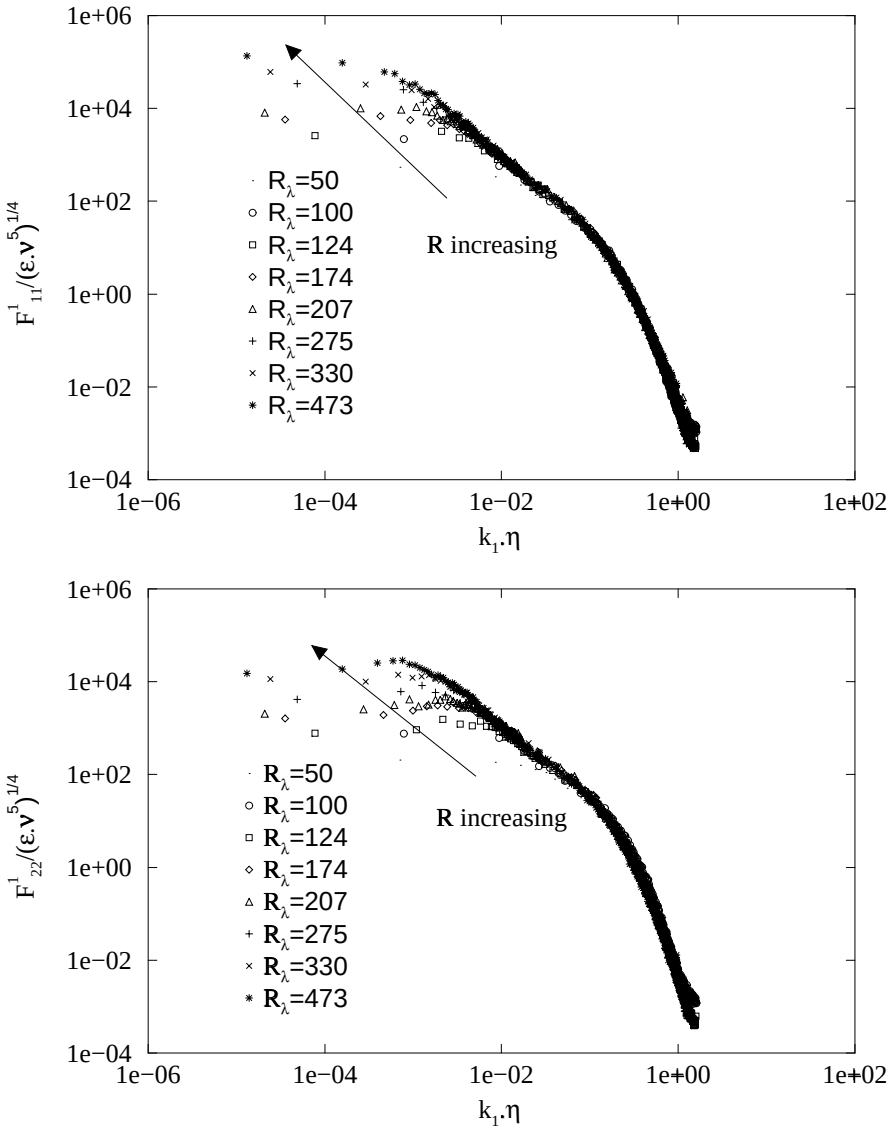

Figure 7.2: One-dimensional spectra in high wavenumber scaling

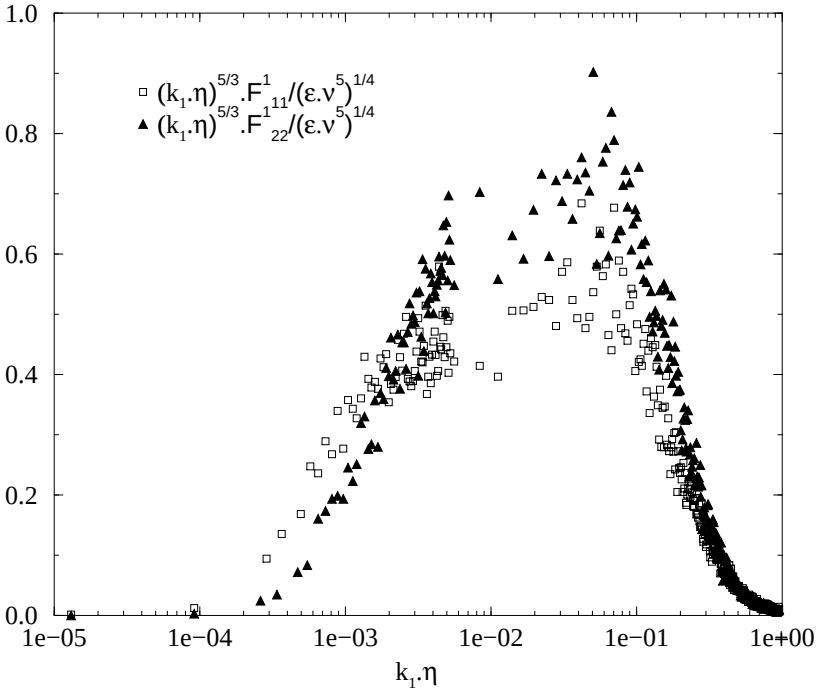

Figure 7.3: One-dimensional spectra in high wavenumber scaling multiplied by $\tilde{k}_1^{5/3}$

Table 7.3: Ratio of the physical integral scale over the pseudo integral scale

R_λ	50	100	124	174	207	275	330	473
L_1/l	1.56	1.17	0.93	0.89	0.79	1.21	0.93	0.82

7.3 The Low Wavenumber Scaling

The low wavenumber scaling (equation 5.4) uses the integral scale defined using equations 4.5 and 4.6 for the one-dimensional half-line spectrum. The main problem was to obtain the value of the spectrum at the origin, since it was not included in the data set. The pseudo-integral scale $l = 0.9u^3/\epsilon$ was given. However, the ratio $L_1/l = \phi$ is Reynolds number dependent (see table 7.3). Therefore, a determination of L_1 and L_2 was essential, but the spectra can not be determined at zero wavenumbers because of record length limitation. Moreover, the spectral errors cannot be removed by smoothing since there are fewer estimates here and the spectrum shape is changing rapidly.

The one-dimensional spectra at the origin ($k_1 = 0$) can be expanded as (see Tennekes and Lumley [32]):

$$F_{11}^1 = A_1 - B_1.k_1^2 + C_1.k_1^4 \tag{7.1}$$

$$F_{22}^1 = A_2 + \frac{1}{2}B_2.k_1^2, \tag{7.2}$$

where $B_1 = B_2$ if isotropic.

By fitting the curves to the measured spectra at the lowest wavenumbers, it was possible to extrapolate the "zero wavenumbers" values without being dependent on simply the lowest wavenumber data alone. The different values of the integral scales can be found in table 7.4.

The low wavenumber scaling is seldom found in the literature, due mainly to the problem of definition of the integral scale. We scaled therefore our spectra with

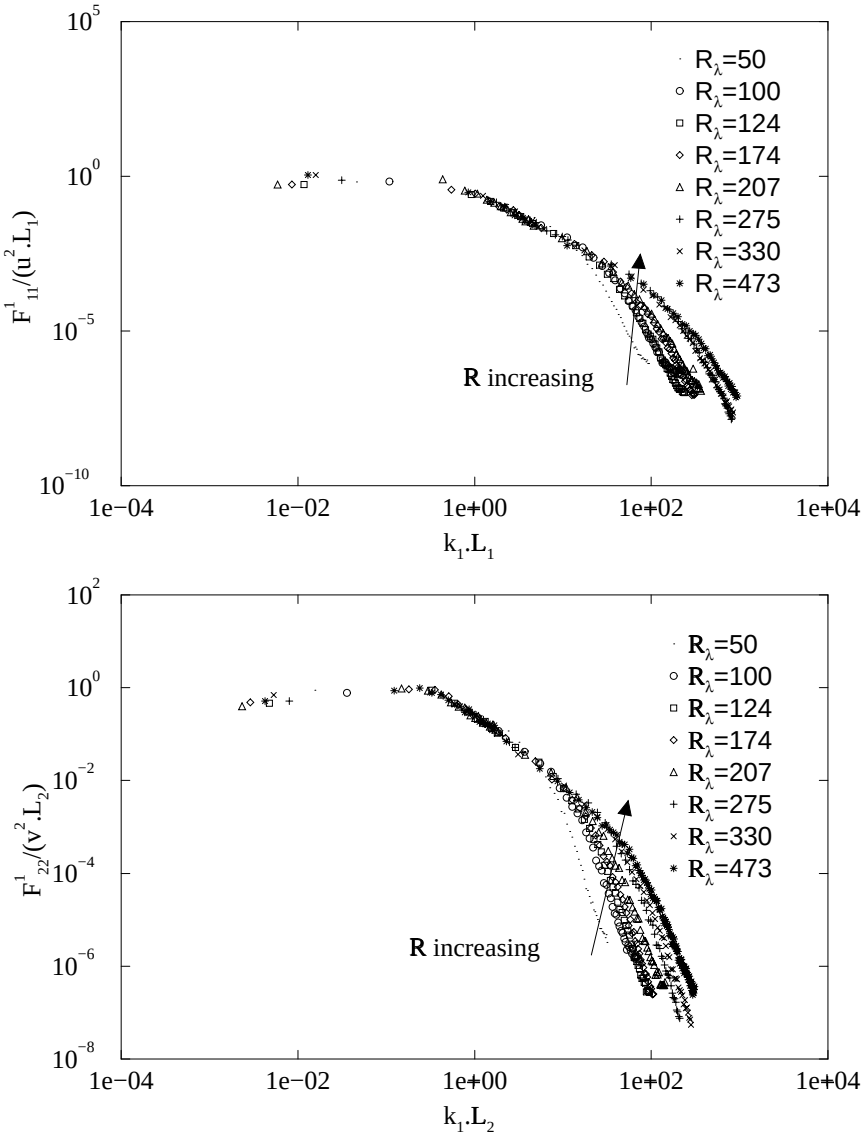

Figure 7.4: One-dimensional spectra in low wavenumber scaling

Table 7.4: The Integral scales

R_λ	50	100	124	174	207	275	330	473
$\mathbf{L_1}$ (m)	0.0226	0.0648	0.0483	0.0532	0.0500	0.1364	0.1054	0.1218
$\mathbf{L_2}$ (m)	0.0076	0.0213	0.0196	0.0180	0.0198	0.0346	0.0356	0.0398

u^2L_1 for the longitudinal part and v^2L_2 for the lateral one. As expected, we see (figure 7.4) a good collapse until the high wavenumber values where the scaling is no longer appropriate. The lowest Reynolds number spectrum does not really show any power-law region, therefore we should expect some problems in finding the correct exponent. The problem with the initial conditions is also present with the lack of a consistent Reynolds numbers' trend at high wavenumbers outside the collapse zone. The phenomenon is the same as for the the high wavenumbers scaling.

To emphasize the fact that the low wavenumber scaling is the most appropriate, we also show the spectra non-dimensionalized with u and $l = 0.9u^3/\epsilon$, the integral scale used by Mydlarski and Warhaft [25] (see figure 7.5), and u and λ (figure 7.6). Although the difference is slight it is still clear that the proper scaling uses the physical integral scale L.

7.4 Direct Determination of μ

As seen, for instance in figure 7.3, the exponent in the power law region is different from $-5/3$; this difference is μ as defined in chapter 6. Mydlarski and Warhaft [25] computed its value by choosing the exponent n such as $k_1^n.F_{ii}^1$ get a constant plateau. Unfortunately, it appears they did not recognize the isotropic properties of the spectrum, and thus, cited two different values for μ: one for the longitudinal part of the spectrum and one for the lateral part. In effect, this reduces by half the amount of data that can be used to account for statistical accuracy. We treated both longitudinal and lateral spectrum together using isotropic assumptions (implying the

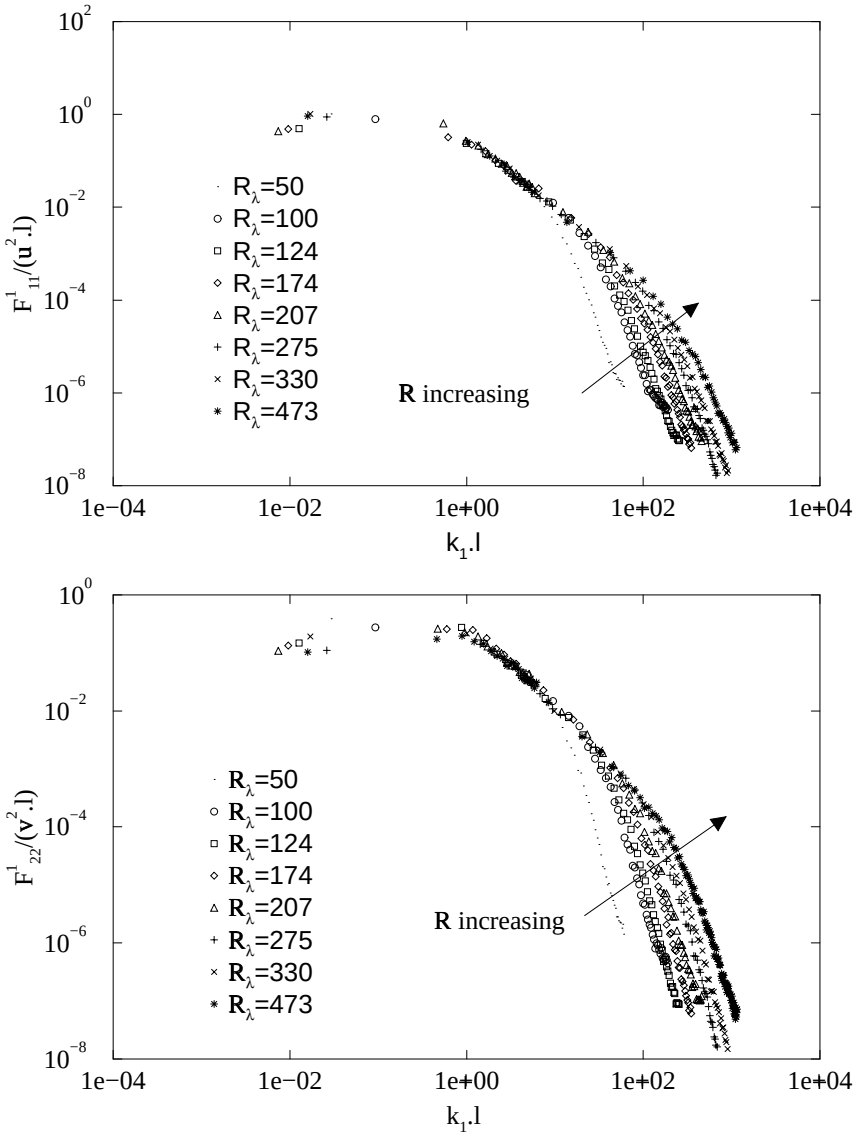

Figure 7.5: One-dimensional spectra scaled with u and l

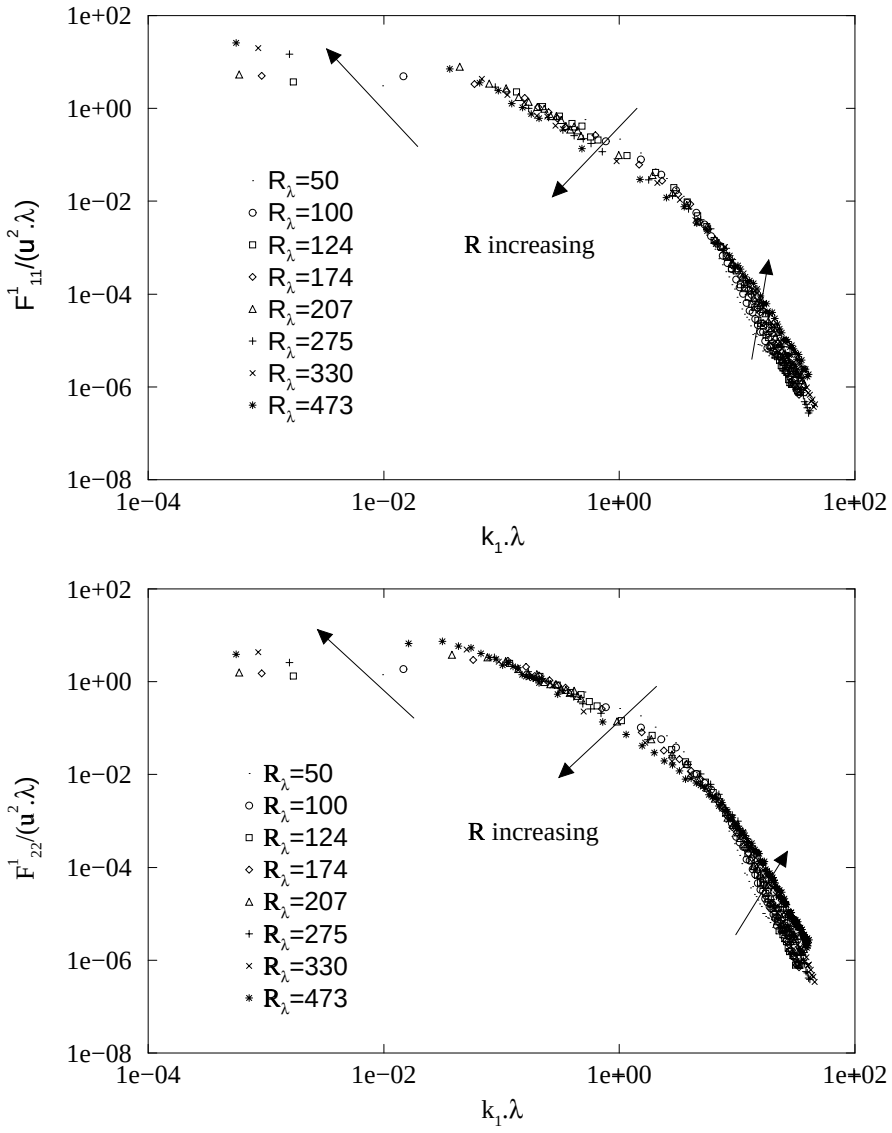

Figure 7.6: One-dimensional spectra scaled with u and λ

same exponent for the two spectra). Once μ is found in this manner, the values of C_{Hi} and C_{Li} are read on the curves of $\tilde{F}^1_{ii}.\tilde{k}_1^{5/3-\mu}$ and $\overline{F}^1_{ii}.\overline{k}_1^{5/3-\mu}$.

Another way to find μ is to use equations 6.20 and 6.21 for the power-law region:

$$\left.\frac{\overline{k}}{f_L}\frac{\partial f_L}{\partial \overline{k}}\right|_R = -5/3 + \mu(R) \tag{7.3}$$

$$\left.\frac{\tilde{k}}{f_H}\frac{\partial f_H}{\partial \tilde{k}}\right|_R = -5/3 + \mu(R). \tag{7.4}$$

So, we now have four different ways of obtaining μ:

- using equations 7.3 or 7.4 (see for instance figure 7.7),
- finding μ such as $k_1^{-5/3+\mu}.F^1_{ii}$ is constant in a region,

and doing it for F^1_{11} and F^1_{22} simultaneously to get the same value of μ for the two one-dimensional spectra. Unfortunately, even with this, due to the scatter (even when using filters), there is much room left in the determination of μ.

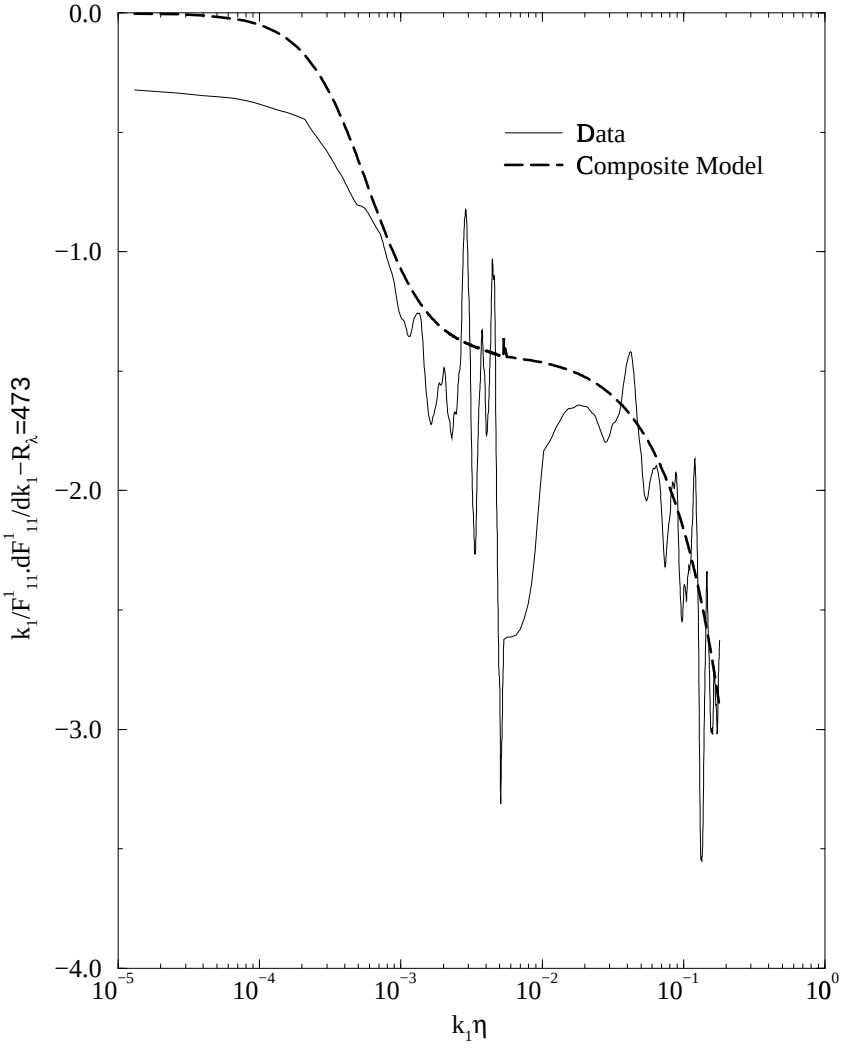

Figure 7.7: Derivation of μ using $\frac{\tilde{k}}{f_H}\frac{\partial f_H}{\partial \tilde{k}} = -5/3 + \mu(R)$ for $R_\lambda = 473$

Chapter 8

Empirical Spectral Models

The main reason for the development of these models is to get a better estimate for $\mu(R)$. As it has been seen in the previous chapter, the scatter of the data set complicates the determination of the Reynolds number dependence of μ. Another problem complicating the determination is that even with no scatter in the data, the overlap region at finite Reynolds number is never completely free from the influence of both the high and low wavenumbers regions. The objective of this chapter is, thus, to develop an analytical model depending only on μ to fit the data set. The primary advantage of this approach is that **all** of the spectral data can be used in the determination of μ, not just that in the overlap region. Thus, there is no arbitrary choice of which data to include in the determination of μ, and which to discard.

It has been customary to consider two classes of spectral models: a low wavenumber one and a high wavenumber one. The low wavenumber model should roll off a $k^{-5/3}$ and never reach the dissipation range. An example is the Von Karman model considered below. The high wavenumber model, on the opposite, starts as $k^{-5/3}$ then rolls off exponentially with increasing wavenumbers. All of the existent models have been developed at infinite Reynolds number, and we must therefore modify those existing models to incorporate the effect of finite Reynolds number. We then mix these two models to create a composite model (in a similar way to Driscoll [4] or Helland,

Van Atta and Stegen [14]) which then covers all the wavenumber range.

8.1 A Low Wavenumber Model

At low wavenumbers, the energy spectrum starts from zero wavenumber as k^n where $1 < n < 4$ (Lesieur [22]). Von Karman and others have gotten reasonable agreement with grid generated turbulence by using $n = 4$ and the following functional form:

$$E(x) = B\frac{x^4}{(1+x^2)^{17/6}} \tag{8.1}$$

With $x = k/k_e$, B and k_e to be defined.

To incorporate the finite Reynolds number form in the matching region, we modify the above model:

$$E(x) = B\frac{x^4}{(1+x^2)^{17/6-\mu/2}}. \tag{8.2}$$

Using this model, we find the functional form for the 1-D longitudinal half-line spectrum:

$$\begin{aligned} \mathcal{F}_{11}^1(k_1) &= \int_{k_1}^{\infty}\left(1-\left(\frac{k_1}{k}\right)^2\right)\cdot\frac{E(k)}{k}\,dk \\ &= \frac{2B}{\left(\frac{11}{3}-\mu\right)\left(\frac{5}{3}-\mu\right)}\left(1+x_1^2\right)^{-5/6+\mu/2}. \end{aligned} \tag{8.3}$$

To define B and k_e we use the relations between u^2 and the integral scale and $\mathcal{F}_{11}^1$, since, at low wavenumbers, u^2 and L_1 are the proper scaling parameters.

$$\begin{aligned} u^2 &= \int_0^{\infty}\mathcal{F}_{11}^1\,dk_1 \\ &= \frac{2Bk_e}{\left(\frac{11}{3}-\mu\right)\left(\frac{5}{3}-\mu\right)}\int_0^{\infty}\left(1+x_1^2\right)^{-5/6+\mu/2}\,dx_1 \\ &= \frac{Bk_e}{\left(\frac{11}{3}-\mu\right)\left(\frac{5}{3}-\mu\right)}\sqrt{\pi}\frac{\Gamma\left(\frac{1}{3}-\frac{\mu}{2}\right)}{\Gamma\left(\frac{5}{6}-\frac{\mu}{2}\right)} \end{aligned} \tag{8.4}$$

where Γ is the Euler-Gamma function.

The definition of the integral scale implies:

$$\begin{aligned} L_1 &= \pi \frac{\mathcal{F}_{11}^1(0)}{2u^2} \\ &= \frac{\pi}{u^2} \cdot \frac{B}{\left(\frac{11}{3}-\mu\right)\left(\frac{5}{3}-\mu\right)}. \end{aligned} \tag{8.5}$$

Combining equations 8.4 and 8.5, we define k_e to be:

$$k_e = \frac{\sqrt{\pi} \cdot \Gamma\left(\frac{5}{6}-\frac{\mu}{2}\right)}{L_1 \cdot \Gamma\left(\frac{1}{3}-\frac{\mu}{2}\right)} \tag{8.6}$$

Finally, equations 8.3 and 8.5 lead to the final form of the low wavenumber model:

$$\mathcal{F}_{11}^1(k_1) = 2\frac{u^2 L_1}{\pi}\left(1+x_1^2\right)^{-5/6+\mu/2} \tag{8.7}$$

$$F_{11}^1(k_1) = \frac{u^2 L_1}{\pi}\left(1+x_1^2\right)^{-5/6+\mu/2}. \tag{8.8}$$

This model is valid for low wavenumber scaling hence, in the limit of infinite wavenumbers, it should go asymptotically towards the matching form of the 1-D spectrum. In the limit $k_1 L_1 \to \infty$ (or $x_1 \to \infty$):

$$\begin{aligned} F_{11}^1 &\to \frac{u^2 L_1}{\pi}\left(\frac{k_1 L_1}{k_e L_1}\right)^{-5/3+\mu} \quad \text{(model limit)} \\ &= u^2\, L_1\, C_{L1}\, (k_1 L_1)^{-5/3+\mu} \quad \text{(power form)} \end{aligned}$$

Clearly these two equations require:

$$C_{L1} = \frac{1}{\pi}\,(k_e L_1)^{5/3-\mu} \tag{8.9}$$

where both μ and C_{L1} depending on the Reynolds number.

8.2 A High Wavenumber Model

There are numerous examples of high wavenumber spectral models. Monin and Yaglom [24], for instance have an exhaustive review. We will consider in this work an improvement of the Lin-Hill model, which seems to reproduce the spectral behavior the best. This model originated from Corrsin and Pao's ([26] and [27]) ideas on modeling S as a function of E and k, in addition to ϵ. Later on, Lin [23] improved the model to better simulate the spectral behavior at high wavenumbers. Finally Hill [15] extended slightly the model. Based on Driscoll [4], we name the final model Lin-Hill.

The dynamical equation for the energy spectrum in isotropic turbulence (see chapter 5) is:

$$\frac{\partial E(k)}{\partial t} = T(k) - 2\nu k^2 E(k). \tag{8.10}$$

This equation reduces for high wavenumbers to:

$$T(k) = 2\nu k^2 E(k). \tag{8.11}$$

T represents the energy transfer between the different wavenumbers, due to nonlinear interactions. An interesting property of T is that the net energy transfer is zero, i.e.:

$$\int_0^\infty T(k)\, dk = 0 \tag{8.12}$$

therefore allowing the definition of an energy flux function (see Batchelor[2]) by:

$$\begin{aligned} \frac{dS(k)}{dk} &= -T(k) \\ &= -2\nu k^2 E(k). \end{aligned} \tag{8.13}$$

We will work in the non-dimensional variables defined in section 5.1:

$$\tilde{k} = k\eta$$

$$\tilde{E} = \frac{E}{(\nu^5 \epsilon)^{1/4}}.$$

The characteristic parameters at high wavenumbers are ϵ and ν. Using the definition of ϵ in terms of the energy spectrum, we can define a constraint equation for the model:

$$\begin{aligned} \epsilon &= 2\nu \int_0^\infty k^2 \, E \, dk \\ &= 2\nu \int_0^\infty \eta^{-2} \, \tilde{k}^2 \, \tilde{E} \, (\nu^5 \, \epsilon)^{1/4} \, \eta^{-1} \, d\tilde{k} \\ 1 &= 2 \int_0^\infty \tilde{k}^2 \tilde{E} \, d\tilde{k}. \end{aligned} \tag{8.14}$$

This ensures that the high wavenumbers spectrum produces the correct dissipation integral.

Adapting the model proposed by Lin in 1978 [15], we propose the functional form for $\tilde{S} = S/\epsilon$:

$$\tilde{S} = \alpha^{-1} \tilde{k}^{5/3-\mu} \frac{\tilde{E}(\tilde{k})}{(1 + (\tilde{k})^{2/3})}. \tag{8.15}$$

Using this model into equation 8.13 (rewritten in non-dimensional variables), we get:

$$\frac{d}{d\tilde{k}} \left(\frac{\tilde{k}^{5/3-\mu} \, \tilde{E}}{(1 + \tilde{k}^{2/3})} \right) = -2 \, \alpha \, \tilde{k}^2 \, \tilde{E}, \tag{8.16}$$

which expands into:

$$\frac{d\tilde{E}}{\tilde{E}} = \left(-2 \, \tilde{k}^{1/3-\mu} \, (1 + \tilde{k}^{2/3}) \, (\alpha) + 2/3 \, \tilde{k}^{-1/3} \, (1 + \tilde{k}^{2/3})^{-1} - (5/3 - \mu) \, \tilde{k}^{-1} \right) d\tilde{k}. \tag{8.17}$$

Integration leads immediately to a functional form for the energy spectrum E:

$$\frac{\tilde{E}}{\tilde{E}_0} = \left(\frac{1 + \tilde{k}^{2/3}}{1 + \tilde{k}_0^{2/3}} \right) \left(\frac{\tilde{k}}{\tilde{k}_0} \right)^{-5/3+\mu} \exp \left[-2\alpha \left(\frac{\tilde{k}^{4/3+\mu} - \tilde{k}_0^{4/3+\mu}}{4/3 + \mu} + \frac{\tilde{k}^{2+\mu} - \tilde{k}_0^{2+\mu}}{2 + \mu} \right) \right] \tag{8.18}$$

where $\tilde{E}_0$ and $\tilde{k}_0$ are integration constants.

To define the constants, we now use the constraint equation 8.14:

$$\frac{(1+\tilde{k}_0^{2/3})\,\tilde{k}_0^{-5/3+\mu}}{2\tilde{E}_0} = \int_0^\infty \left(\tilde{k}^{1/3+\mu} + \tilde{k}^{1+\mu}\right) \exp\left[-2\alpha\left(\frac{\tilde{k}^{4/3+\mu} - \tilde{k}_0^{4/3+\mu}}{4/3+\mu} + \frac{\tilde{k}^{2+\mu} - \tilde{k}_0^{2+\mu}}{2+\mu}\right)\right] d\tilde{k} \tag{8.19}$$

Recognizing in the integral the form "$f' \cdot exp(f)$" leads to:

$$\frac{(1+\tilde{k}_0^{2/3})\,\tilde{k}_0^{-5/3+\mu}}{\tilde{E}_0} = \frac{1}{\alpha} \exp\left[2\alpha\left(\frac{\tilde{k}_0^{4/3+\mu}}{4/3+\mu} + \frac{\tilde{k}_0^{2+\mu}}{2+\mu}\right)\right] \tag{8.20}$$

implying a relation between $\tilde{E}_0$ and $\tilde{k}_0$:

$$\tilde{E}_0 = \alpha\,(1+\tilde{k}_0^{2/3})\,\tilde{k}_0^{-5/3+\mu} \exp\left[-2\alpha\left(\frac{\tilde{k}_0^{4/3+\mu}}{4/3+\mu} + \frac{\tilde{k}_0^{2+\mu}}{2+\mu}\right)\right]. \tag{8.21}$$

Using the latest equation into the functional form of the energy spectrum (equation 8.18) leads finally to a completely defined analytical model:

$$\tilde{E} = \alpha\,(1+\tilde{k}^{2/3})\,\tilde{k}^{-5/3+\mu} \exp\left[-2\alpha\left(\frac{\tilde{k}^{4/3+\mu}}{4/3+\mu} + \frac{\tilde{k}^{2+\mu}}{2+\mu}\right)\right]. \tag{8.22}$$

Since the model reduces to the overlap power law form when $\tilde{k} \to 0$, we can identify α as C_H. Note that C_H (or α) and μ depend on Reynolds number.

Finally, using the isotropic relation between $\mathcal{F}_{11}^1$ and E (equation 3.27), we can implement the model for $\mathcal{F}_{11}^1$. Unfortunately, there is no analytical solution as for the low wavenumber case, and a numerical integration has to be performed instead.

8.3 A Composite Model

We now have two models that define two different scaling regions, and overlap in a common one (see figure 8.1). We can now build a composite model to describe the spectrum in the whole range of wavenumbers by combining these two models. To

accomplish this, we have two possibilities:

- Additive Composite Model:

  We define the composite model as the sum of the low wavenumber and the high wavenumber models and subtract the overlap power form, which is the common part. This common part can be expressed in either low or high wavenumbers form, i.e.:

$$E_{composite} = (u^2 L)\,\overline{E}_{Lowwave}(\overline{k}) + (\epsilon\nu^5)^{1/4}\,\tilde{E}_{Highwave}(\tilde{k}) - (u^2 L)\,C_L\,(\overline{k})^{-5/3+\mu} \tag{8.23}$$

  Or:

$$E_{composite} = (u^2 L)\,\overline{E}_{Lowwave}(\overline{k}) + (\epsilon\nu^5)^{1/4}\,\tilde{E}_{Highwave}(\tilde{k}) - (\epsilon\nu^5)^{1/4}\,C_H\,(\tilde{k})^{-5/3+\mu}$$

- Multiplicative Composite Model:

  We define the composite model as the product of the low wavenumber and the high wavenumber models and divide by the common part. This type of model has been developed, for instance, by Helland *et al* [14]. Again, there are two ways of expressing the common part so:

$$E_{composite} = \frac{(u^2 L)\,\overline{E}_{Lowwave}(\overline{k}) * (\epsilon\nu^5)^{1/4}\,\tilde{E}_{Highwave}(\tilde{k})}{(u^2 L)\,C_L\,(\overline{k})^{-5/3+\mu}} \tag{8.24}$$

  Or:

$$E_{composite} = \frac{(u^2 L)\,\overline{E}_{Lowwave}(\overline{k}) * (\epsilon\nu^5)^{1/4}\,\tilde{E}_{Highwave}(\tilde{k})}{(\epsilon\nu^5)^{1/4}\,C_H\,(\tilde{k})^{-5/3+\mu}}$$

  We will see that only the multiplicative form leads to a useful result because of the singularity in the high wavenumber modified Lin-Hill model when $\tilde{k} \to 0$.

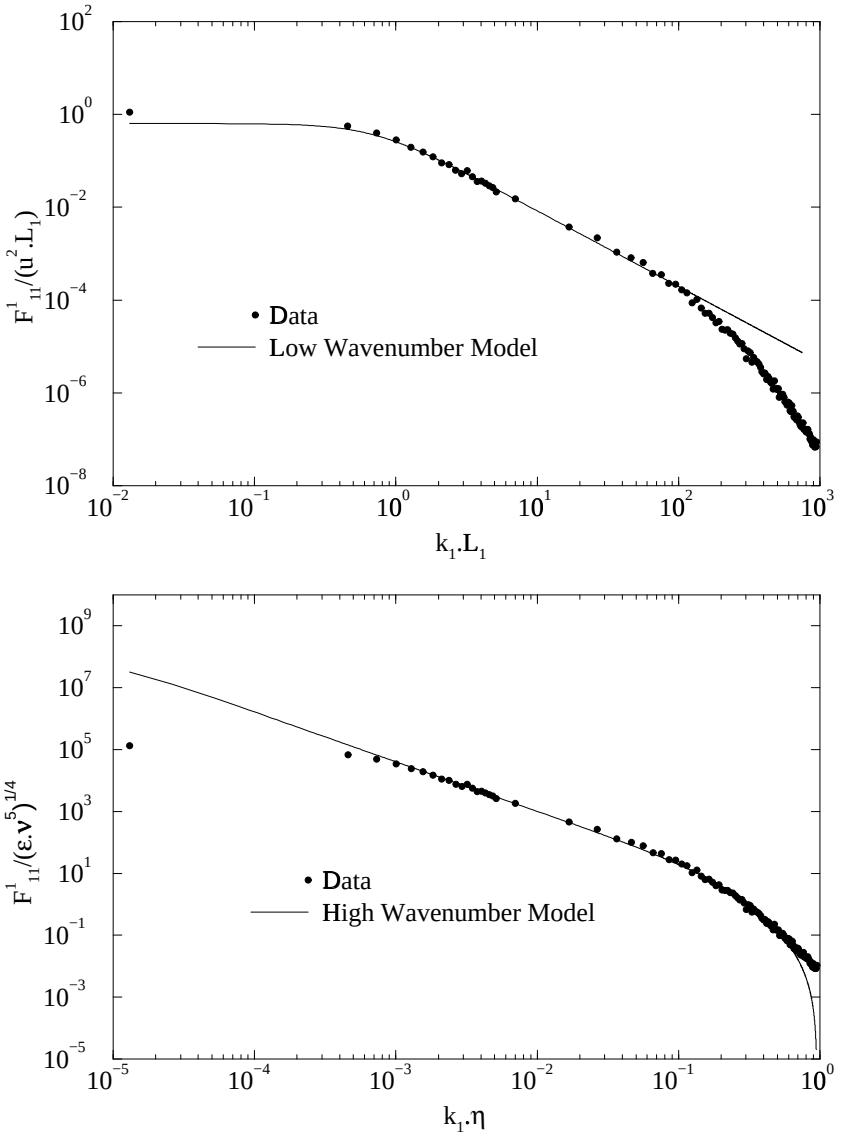

Figure 8.1: Low and high wavenumber models implemented separately at $R_\lambda = 473$

The basic form for the low wavenumber model was

$$\overline{E}(\overline{k}) = \overline{B}\,\frac{(\overline{k}/\overline{k}_e)^4}{(1+(\overline{k}/\overline{k}_e)^2)^{17/6-\mu/2}}$$

and for the high wavenumber model:

$$\frac{\tilde{E}}{\tilde{E}_0} = \left(\frac{1+\tilde{k}^{2/3}}{1+\tilde{k}_0^{2/3}}\right)\left(\frac{\tilde{k}}{\tilde{k}_0}\right)^{-5/3+\mu} \exp\left[-2\alpha\left(\frac{\tilde{k}^{4/3+\mu}-\tilde{k}_0^{4/3+\mu}}{4/3+\mu}+\frac{\tilde{k}^{2+\mu}-\tilde{k}_0^{2+\mu}}{2+\mu}\right)\right].$$

Note: We can not simply use the low and high wavenumber models separately since we introduced μ to account for finite Reynolds number effects, and their respective roll offs are infinite Reynolds number effects due to a total separation between the dissipation and the production ranges.

As it has been seen in the previous chapter, the two models have been set up by using three different constraint equations:

1. The integral scale (equation 4.7):

$$L_1 = \frac{3\pi}{4}\frac{\int_0^\infty E(k)/k\,dk}{\int_0^\infty E(k)\,dk}$$

2. The dissipation rate (equation 3.25):

$$\epsilon = 2\nu\int_0^\infty k^2 E(k)\,dk$$

3. The relation with u^2 (equation 3.7):

$$\frac{3}{2}u^2 = \int_0^\infty E(k)\,dk$$

But, those equations have been used on either one of the models and not on the composite model. So the constants found for those models by using the constraints equations are not valid for a composite model. To define these constants in a composite model, the three constraint equations should be applied to the composite model itself. Unfortunately, due to the special form of the high wavenumber model, the constraint equation number 1 can not be used in the additive version since the result of the integration is not finite. So, an additive composite model can not be rigorously defined.

For the multiplicative composite spectrum, however, all integrals are defined, and thus the problem encountered by the additive composite spectrum vanishes. However, the integrals do not have an analytical solution, and so we must carry out all integrations numerically.

8.4 Implementation of the Composite Model

As defined in chapter 8.3, we developed a multiplicative composite spectrum. We first kept the values of μ found with the data alone (see chapter 7.4), and allowed the different constants in the model to vary to verify the three constraint equations altogether[1]. This allowed the model to initialize the constants for the next search based on the value of μ found with the data. The next step was to allow all the constants and μ to change to optimize the fit with the data while still verifying the constraint equations. The graphical results are shown in figures 8.2 and 8.3.

The values for μ (see chapter 9) were quite close to the ones found with the data analysis alone, thus reassuring us of their validity. The only major discrepancies were for $R_\lambda = 50$ and $R_\lambda = 275$. The last one was not really isotropic (see chapter 7.1) and since we used an isotropic relation to relate the energy spectrum to the one-dimensional the result is not surprising. The lowest Reynolds number ($R_\lambda = 50$) was

[1] All optimization schemes in this thesis were done with Microsoft Excel solver constrained to reduce the sum of absolute errors between the model and the data values.

Table 8.1: Composite values

R_λ	50	100	124	174	207	275	330	473
μ	0.13	0.19	0.18	0.14	0.13	0.02	0.09	0.11
C_{L1}	0.439	0.350	0.302	0.322	0.308	0.426	0.345	0.312
C_{L2}	0.387	0.291	0.282	0.259	0.279	0.328	0.279	0.282
C_{H1}	0.589	0.798	0.830	0.805	0.812	0.453	0.700	0.799
C_{H2}	0.773	1.026	1.005	1.045	1.043	0.606	0.938	1.008

also the only value that did not fit into the analytical model for μ as developed in chapter 9.1. So it is our opinion that there is no real overlap region at $R_\lambda = 50$ (we should note that this Reynolds number is quite far from the "sufficiently large Reynolds number" necessary to the inertial subrange from Kolmogorov). The values for the other Reynolds numbers are remarkably close to those determined graphically as described earlier.

Once μ was defined, we found the values of C_H and C_L the same way we found them with the data analysis by multiplying the spectra by $\tilde{k}^{5/3-\mu}$ and $\overline{k}^{5/3-\mu}$ respectively. We did it for the data and the composite spectra and found similar values (see table 8.1).

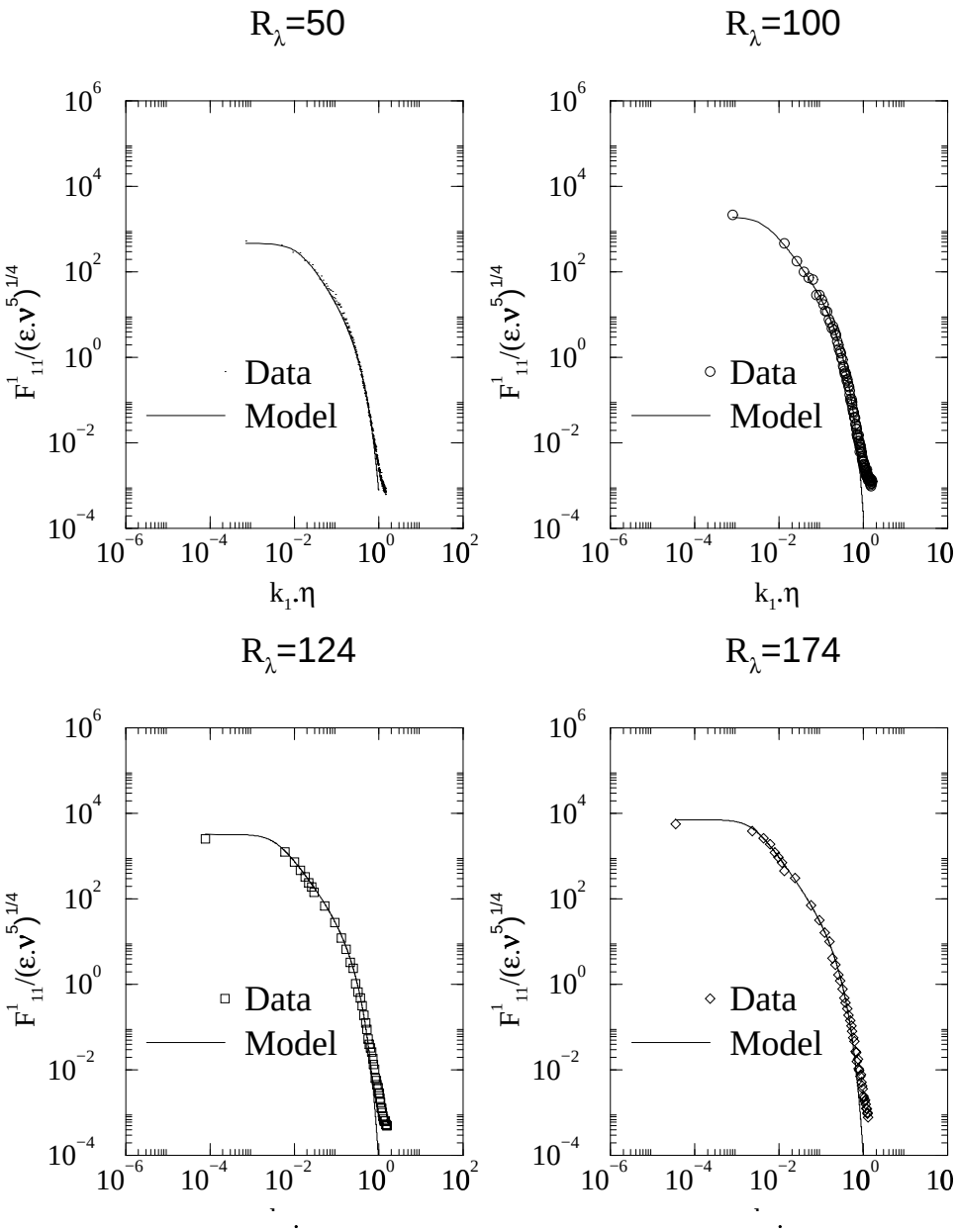

Figure 8.2: The composite model for the first four Reynolds numbers

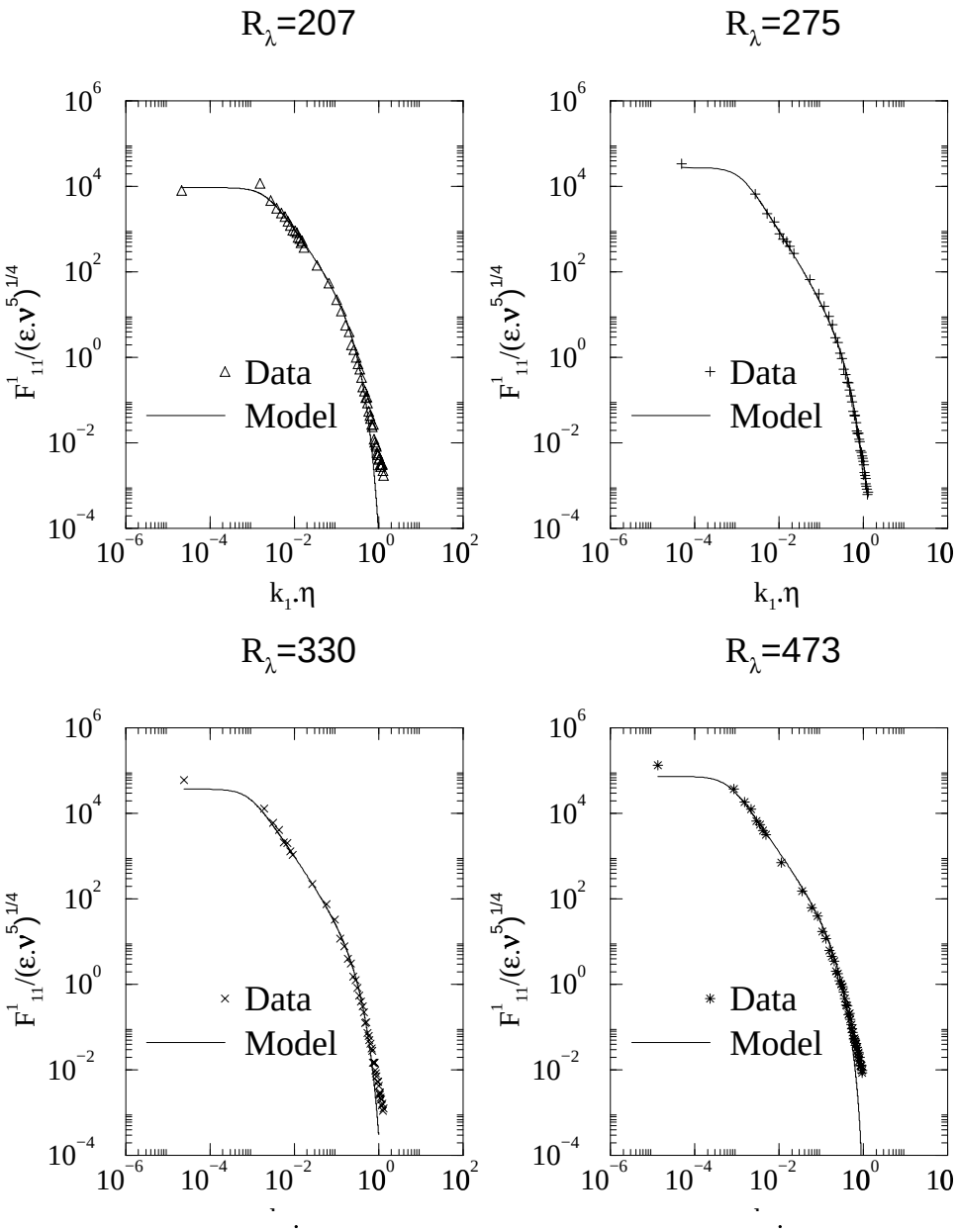

Figure 8.3: The composite model for the last four Reynolds numbers

Chapter 9

Conclusive Remarks on μ

We saw in chapter 6 that to fully define the spectrum in the overlap region, we needed a functional form for h, that is directly linked to μ.

9.1 A model for $\mu(R)$

The only "free" function is h. Based on George and Castillo (1997) [10], we propose a model of the form:

$$h - h_\infty = \frac{A}{(\ln R)^\beta}. \tag{9.1}$$

for which, the only adjustable parameters are A and β.

Substituting the model into equation 6.28:

$$\mu = \gamma - \gamma_\infty = \frac{\beta A}{(\ln R)^{\beta+1}}. \tag{9.2}$$

Equations 6.27 and 6.30 yield:

$$\begin{aligned} \frac{C_H}{C_L} &= \exp\left((\gamma - \gamma_\infty)\ln R + h\right) \\ &= \frac{C_{H\infty}}{C_{L\infty}} \exp\left(\frac{(\beta+1)A}{(\ln R)^\beta}\right). \end{aligned} \tag{9.3}$$

Table 9.1: Values of μ found by different ways

$R^{\smile}$	Present Work		Warhaft and Mydlarski	
	Data analysis	**Composite spectrum**	$\boldsymbol{\mu_1}$	$\boldsymbol{\mu_2}$
50	0.43	0.13	0.37	0.57
100	0.19	0.19	0.37	0.37
124	0.18	0.18	0.17	0.27
174	0.14	0.14	0.15	0.21
207	0.13	0.13	0.15	0.21
275	0.11	0.02	0.13	0.21
330	0.11	0.09	0.11	0.15
473	0.11	0.11	0.09	0.11

Also:

$$\begin{aligned}\frac{f_L}{f_H} &= g(R) = \frac{C_{L\infty}}{C_{H\infty}} \exp\left(-\frac{(\beta+1)A}{(\ln R)^\beta} + \gamma \ln(R)\right) \\ &= \frac{C_{L\infty}}{C_{H\infty}} \exp\left(-\frac{(\beta+1)A}{(\ln R)^\beta} + \frac{(\beta)A}{(\ln R)^\beta} + \gamma_\infty \ln(R)\right) \\ &= \frac{C_{L\infty}}{C_{H\infty}} R^{\gamma_\infty} \exp\left(-\frac{\beta A}{(\ln R)^\beta}\right). \end{aligned} \tag{9.4}$$

If we examine conditions for the existence of finite $C_{H\infty}$ and $C_{L\infty}$, we find that $\beta > 0$, this possibility rules out Barenblatt and Chorin's [1] proposition where $\beta = 0$.

9.2 Results

Apart from the values found by Mydlarski and Warhaft [25], we have two different ways of having μ:

- Numerical results from a direct data analysis (chapter 7.4)
- Results from the application of the composite model (chapter 8.4)

Results are found in table 9.1.

The model defined in chapter 9.1:

$$\mu = \frac{\beta A}{(\ln R)^{\beta+1}}$$

was then applied to the values found for μ, C_{Hi}, and C_{Li}. Then the model values were implemented back to the data until a reasonable agreement was found between the models and the data. We found the model constants to be:

$$\boxed{\begin{aligned} \boldsymbol{A} &= \mathbf{4.22} \\ \boldsymbol{\beta} &= \mathbf{0.87} \end{aligned}} \tag{9.5}$$

giving the best fit model for μ:

$$\boxed{\boldsymbol{\mu(R) = \frac{3.69}{(\ln R)^{1:87}}}} \tag{9.6}$$

This model has also been applied to the composite values and the differences are negligible. Those values are in table 9.2.

It should be noted however that the values for $R_\lambda = 50$ are suspicious since we did not see any real power law region.

Table 9.2: Implementation of the model for μ

$\boldsymbol{R_\lambda}$	**50**	**100**	**124**	**174**	**207**	**275**	**330**	**473**
$\boldsymbol{\mu}$	0.43	0.19	0.18	0.14	0.13	0.11	0.11	0.11
$\mathbf{C_{L1}}$	0.310	0.351	0.301	0.321	0.308	0.341	0.332	0.312
$\mathbf{C_{L2}}$	0.315	0.292	0.282	0.259	0.278	0.284	0.272	0.282
$\mathbf{C_{H1}}$	1.475	0.793	0.840	0.807	0.815	0.665	0.771	0.797
$\mathbf{C_{H2}}$	1.620	1.021	1.015	1.046	1.047	0.835	1.016	1.005

Figure 9.1 shows the different values of μ found with the data analysis, the composite models and the model applied to μ (chapter 9.1). This model is the best fit to the data, however, George *et al.* [11] found surprisingly that a value of $\beta = 0.44$ was a good fit to similarity analysis to pipe flows, and boundary layers, without being able yet to find the possible consequence of this. We therefore decided to include this model into figure 9.1 to see its eventual fit. We also added Barenblatt and Chorin's hypothesis [1] to emphasize its non-fit, even though their proposition gives infinite values of C_H and C_L in the limit of infinite Reynolds number, and so is not physically acceptable since it contradicts both Kolmogorov and Von Karman simultaneously in the limit. The figure also includes earlier values found by Mydlarski and Warhaft [25] for the longitudinal one-dimensional spectrum, values for the lateral one being too different from ours have not been included.

Figure 9.2 shows C_H/C_L function of R for the two one-dimensional spectra. The scatter in the values is due to the fact that the coefficient C_L (or C_H) is dependent on the value of μ: a small change in μ can give an important difference in the value of C. Clearly the theory and the proposed model are both consistent with the experimental data and reduces to the correct limits.

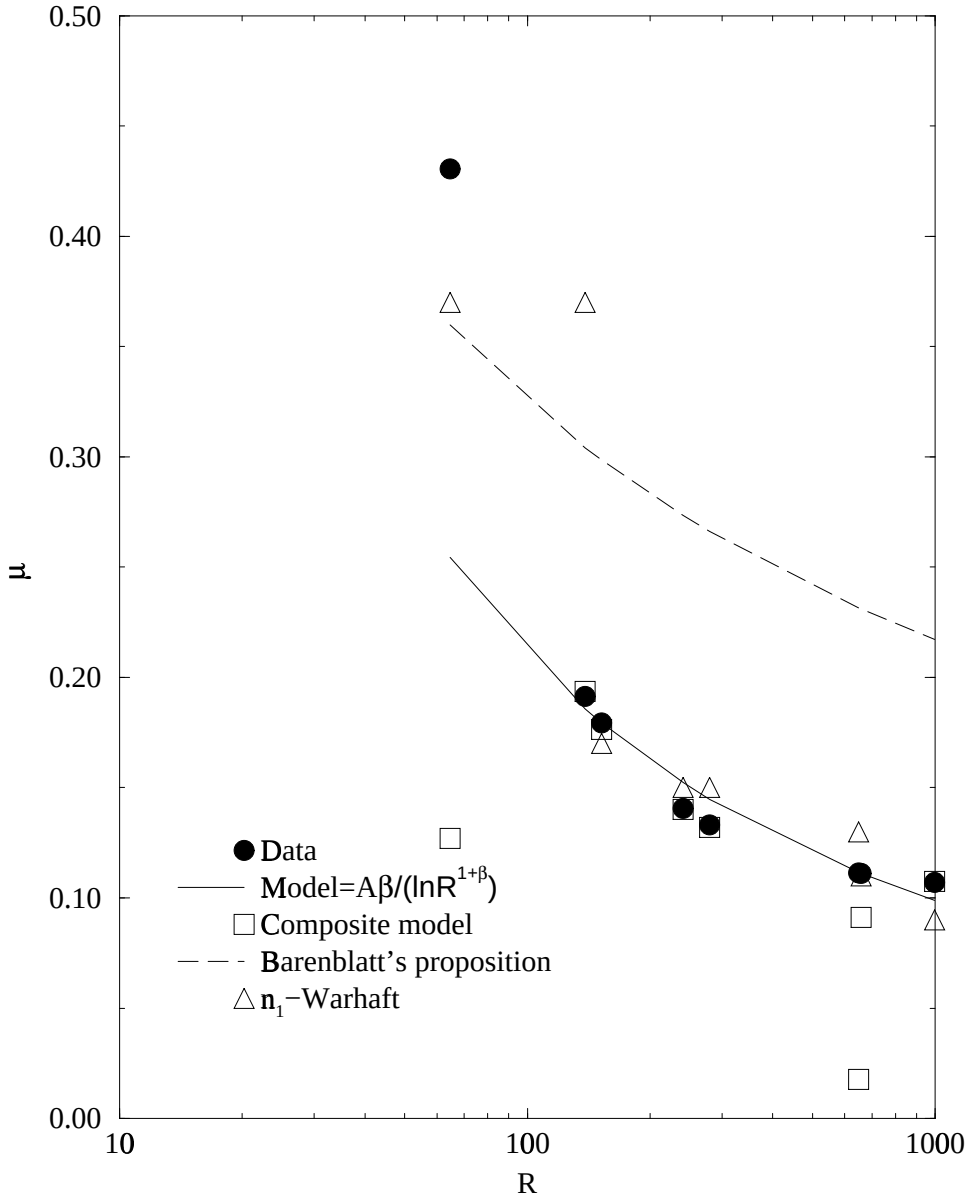

Figure 9.1: Comparison between the values of μ found in different ways

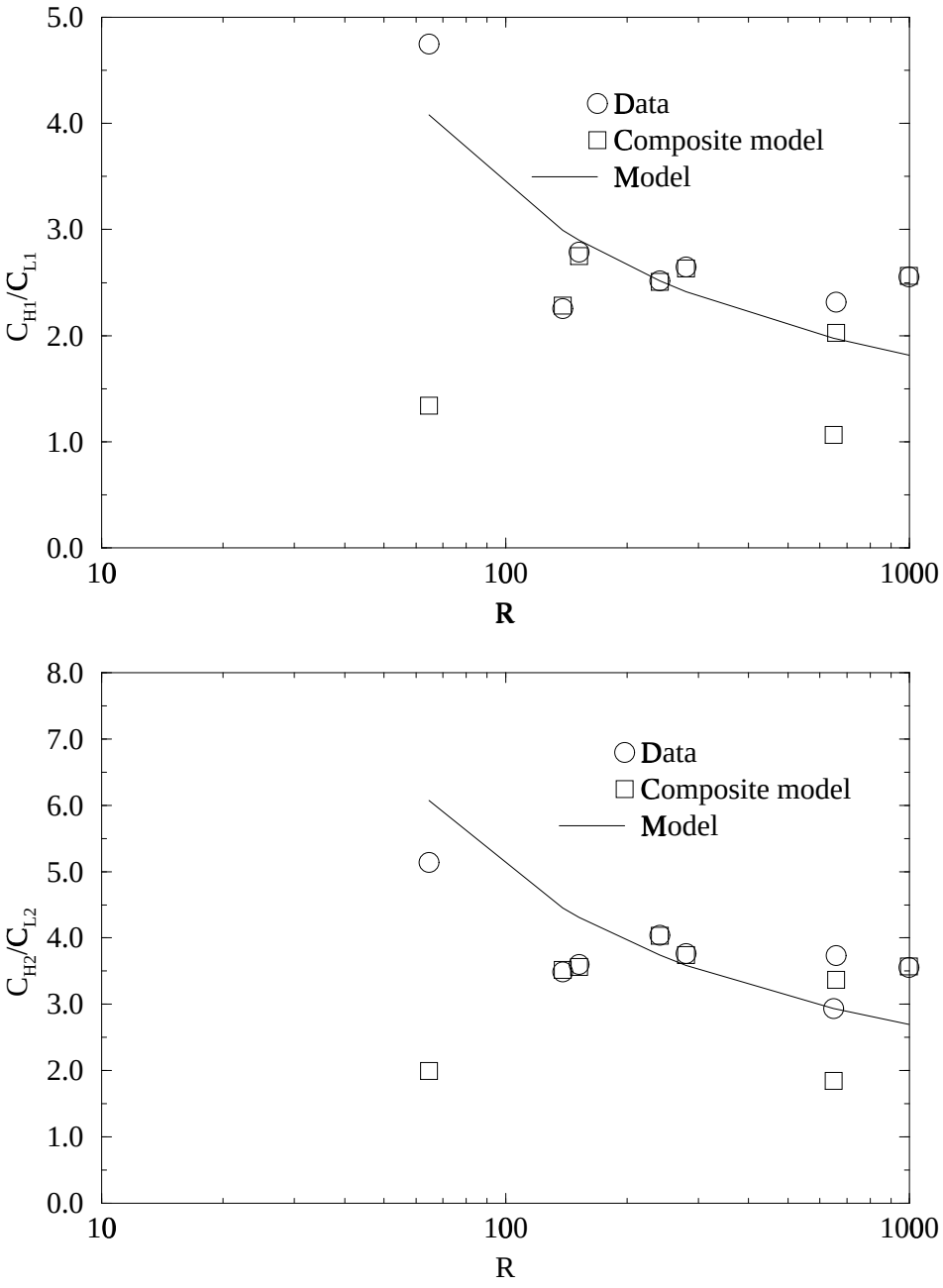

Figure 9.2: Comparison between the values of C_H/C_L found in different ways

Chapter 10

Summary and Conclusions

10.1 Thesis Summary

In the previous pages, we developed a similarity theory for the energy spectrum at finite Reynolds numbers. The aim is to cover the gap before the very large Reynolds numbers where Kolmogorov's hypotheses apply. Since the small scales of turbulence are considered isotropic, we use isotropic simplifications in defining the energy and the one-dimensional spectra. We then consider two ranges of wavenumbers (classified as high and low), and define the appropriate length scales for each region: the so-called Kolmogorov scale, η, which is representative of the small scales in turbulence, and the physical integral scale, that we believe is the appropriate length scale for the low wavenumbers region.

Based on the energy equation

$$\frac{\partial E(k)}{\partial t} = T(k) - 2\nu k^2 E(k)$$

and on its evolution at infinite Reynolds numbers, we derive the appropriate parameters for the two regions. Those parameters are u and ϵ for the low wavenumber region (also being the region containing the energy), and ν and ϵ for the high wavenumber

one (being the dissipation region). With those four parameters, we can collapse the spectrum with scalings from the two regions, while still keeping functions describing the whole range of wavenumbers, at least at finite Reynolds number.

Knowing that the two differently scaled energy spectra still represent the same spectral function, we are able to determine conditions and properties of an overlap region between the two similarity functions, that survives in the limit of an infinite Reynolds number. We prove that the spectrum should follow a power law, k^n, in the overlap. The exponent, $n = -5/3 + \mu$, is Reynolds number dependent but goes to $-5/3$ in the limit of infinite Reynolds number, as predicted by Kolmogorov's hypotheses.

To verify the above theory, we needed a set of data which should be on a wide range of Reynolds numbers, isotropic, and done with nearly same initial conditions, since the functional forms of the spectrum depend largely on it (and is not universal as widely thought). We therefore used data of Mydlarski and Warhaft (1996) [25], that were the closest ones to our request. Unfortunately, these were not always fully isotropic, nor done with the same initial conditions and this has some repercussions on some results. When plotted in either low or high wavenumbers variables, we find a new perfect collapse, proving that the appropriate length scale for low wavenumbers is really the physical integral scale L, and that the exponent is indeed Reynolds number dependent. Using the functional model for μ, we are able to define completely the functional form of the spectrum in the overlap region.

The data, however, contained some scatter, and left some doubts concerning the values of μ. We therefore developed an empirical spectral model allowing a Reynolds number dependent exponent in the overlap region, as stated in the present theory. To do so we created a multiplicative composite spectrum, based on a low wavenumber model extended from a Von Karman one, and on a high wavenumber one, extended from a Lin-Hill version. This composite model was then applied on the data sets for a better evaluation of μ. The results mostly confirm the previous estimates, apart

from the sets that were the farther from our specifications.

We then conclude on the results for μ. We implemented a semi-empirical model for μ, the only "free" choice to completely define the spectrum in the overlap, based on previous works. The model proposed by Barenblatt and Chorin [1] has been found deficient, both because it does not agree with the data, and also because it violates Kolmogorov similarity in the infinite Reynolds number limit.

It is our belief that this methodology can be easily applied to other sets, even non isotropic ones to, perhaps, find a generic functional form for the overlap region, and can certainly be extended to fully define the spectrum as a whole.

10.2 Suggestions for Future Work

We see two main directions for improving the present work. First, on an experimental basis, this theory should be tested on more data sets, providing they are done with same initial conditions, isotropic (unless this theory is expanded on non-isotropic sets, which is certainly possible), and on a sufficient wide range of Reynolds numbers. It should then be interesting to compare the results with the present work to see an eventual common trend. Second, a major problem in this work is the modeling of μ. We decided on an empirical model based on works not really related to this one. Due to certain computer improvements (like genetic algorithms), an optimal functional form of μ can be found that could certainly out-passes the present one. Also, this exponent has also been introduced to take into account intermittency (see for instance Hunt and Vassilicos [17]), and models (like log-normal law proposed by Kolmogorov [21], see Frisch [5] which is more like a prelude to his book [6]) have been developed for that purpose. It could be interesting to see how they adapt to our function.

Another area of improvement lies in the theoretical part. This theory is just a beginning, and consequences should be explored. For instance, the function $\phi = \epsilon L/u^3$ which is the ratio of the physical length scale over the "pseudo" length scale goes to

a constant as the Reynolds number reaches infinite values. Knowing this can lead to a model for ϵ, which would certainly appeal to people using "k-ϵ" models. Also the functional form of the spectrum in either scaling form outside the matching region is still unknown and the conditions of application of an overlap are not really practically clear. Finally, this work is another successful use of the Asymptotic Invariance Principle, and it is logical to continue to find other applications.

References

[1] G. I. Barenblatt and A. J. Chorin. New perspectives in turbulence: Scaling laws, asymptotics and intermittency. *SIAM rev.*, 40(2):265–291, 1998.

[2] G. K. Batchelor. *The Theory of Homogeneous Turbulence.* Cambridge University Press, Cambridge, UK, 1953.

[3] P. Bradshaw. Turbulence: The chief oustanding difficulty of our subject. *Experiments. in Fluids*, 16:203–216, 1994.

[4] R. J. Driscoll. *The Influence of Spectral Transfer and Molecular Diffusion on Turbulent Mixing and Combustion.* PhD thesis, SUNY at Buffalo, 1982.

[5] U. Frisch. From global scaling, à la kolmogorov, to local multifractal scaling in fully developed turbulence. *Proc. R. Soc. Lond. A*, 434:89–99, 1991.

[6] U. Frisch. *Turbulence.* Cambridge University Press, Cambridge, UK, 1995.

[7] W. K. George. The self-preservation of turbulent flows and its relation to initial conditions and coherent structures. In *Advances in Turbulence*, pages 39–73. Hemisphere, NY, 1989.

[8] W. K. George. The decay of homogeneous isotropic turbulence. *Physics of Fluids A*, 4(7):1492–1509, 1992.

[9] W. K. George. Some new ideas for similarity of turbulent shear flows. In *Proc. of Turbulence, Heat and Mass Transfer Symposium*, Lisbon, Portugal, 1994.

[10] W. K. George and L. Castillo. Zero-pressure-gradient turbulent boundary layer. *Applied Mech. Rev.*, 50:689–729, 1997.

[11] W. K. George, L. Castillo, and M. Wosnik. A theory for turbulent pipe and channel flows. *Theoretical and Applied Mechanics*, 1997.

[12] W. K. George and M. M. Gibson. The self-preservation of homogeneous shear flow turbulence. *Experiments in Fluids*, 13:229–238, 1992.

[13] W. K. George and H. J. Hussein. Locally axissymmetric turbulence. *Journal of Fluid Mechanics*, 233:1–23, 1991.

[14] K. N. Helland, C. W. Van Atta, and G. R. Stegen. Spectral energy transfer in high reynolds number turbulence. *Journal of Fluid Mechanics*, 79:337–359, 1977.

[15] R. J. Hill. Models of the scalar spectrum for turbulent advection. *Journal of Fluid Mechanics*, 88:541–562, 1978.

[16] J. O. Hinze. *Turbulence*. McGraw-Hill, New York, NY, 1975.

[17] C. R. Hunt and J.C. Vassilicos. Kolmogorov's contributions to the physical and geometrical understanding of small-scale turbulence and recent developments. *Proc. R. Soc. Lond. A*, 434:183–210, 1991.

[18] T. Von Karman and C. C. Lin. On the concept of similarity in the theory of isotropic turbulence. In *Turbulence: Classical Papers on Statistical Theory*, pages 179–187. Interscience, NY, 1962.

[19] A. N. Kolmogorov. Dissipation of energy in the locally isotropic turbulence. *C. R. Acad. Sci. U.R.S.S.*, 32:16, 1941.

[20] A. N. Kolmogorov. The local structure in incompressible viscous fluids for very large reynolds numbers. *C. R. Acad. Sci. U.R.S.S.*, 30:301, 1941.

[21] A. N. Kolmogorov. A refinement of previous hypotheses concerning the local structure of turbulence in a viscous incompressible fluid at high reynolds number. In *Colloque International du C.N.R.S. de Mécanique de la Turbulence*, Marseilles, France, 1961.

[22] M. Lesieur. *Turbulence in Fluids*. Kluwer Academic Publishers, Boston, MA, 1990. Second Revised Edition.

[23] J. T. Lin. Velocity spectrum of locally isotropic turbulence in the inertial and dissipation ranges. *The Physics of Fluids*, 15:205–207, 1972.

[24] A. S. Monin and A. M. Yaglom. *Statistical Fluid Mechanics*, volume II. MIT Press, Cambridge,MA, 1975.

[25] L. Mydlarski and Z. Warhaft. On the onset of high-reynolds-number grid-generated wind tunnel turbulence. *Journal of Fluid Mechanics*, 320:331–368, 1996.

[26] Y.-H. Pao. Structure of turbulent velocity and scalar fields at large wavenumbers. *The Physics of Fluids*, 8:1063–1075, 1965.

[27] Y.-H. Pao. Transfer of turbulent energy and scalar quantities at large wavenumbers. *The Physics of Fluids*, 11:1371–1372, 1967.

[28] S. G. Saddoughi. Local isotropy in complex turbulent boundary layers at high reynolds number. *Journal of Fluid Mechanics*, 348:201–245, 1997.

[29] S. G. Saddoughi and S. V. Veeravalli. Local isotropy in turbulent boundary layers at high reynolds number. *Journal of Fluid Mechanics*, 268:333–372, 1994.

[30] G. I. Taylor. Statistical theory of turbulence. *Proc. R. Soc. Lond. A*, 151:18–51, 1935.

[31] G. I. Taylor. The spectrum of turbulence. *Proc. R. Soc. Lond. A*, 164:100–114, 1938.

[32] H. Tennekes and J. L. Lumley. *A First Course in Turbulence.* MIT Press, Cambridge,MA, 1972.